



Contents lists available at ScienceDirect

## Journal of Quantitative Spectroscopy &amp; Radiative Transfer

journal homepage: [www.elsevier.com/locate/jqsrt](http://www.elsevier.com/locate/jqsrt)

## Validation of the HITRAN 2016 and GEISA 2015 line lists using ACE-FTS solar occultation observations

K.S. Olsen<sup>a,\*</sup>, C.D. Boone<sup>b</sup>, G.C. Toon<sup>c</sup>, F. Montmessin<sup>a</sup>, A.A. Fedorova<sup>d</sup>, O. Korablev<sup>d</sup>, A. Trokhimovskiy<sup>d</sup><sup>a</sup> Laboratoire Atmosphères, Milieux, Observations Spatiales (LATMOS), Université Versailles St Quentin en Yvelines, Guyancourt 78280, France<sup>b</sup> Department of Chemistry, University of Waterloo, Waterloo, ON N2L 3G1, Canada<sup>c</sup> Jet Propulsion Laboratory (JPL), California Institute of Technology, Pasadena, CA 91109, USA<sup>d</sup> Space Research Institute (IKI), Russian Academy of Sciences, Moscow 117997, Russia

## ARTICLE INFO

## Article history:

Received 18 June 2019

Revised 29 July 2019

Accepted 29 July 2019

Available online 30 July 2019

## Keywords:

ACE-FTS

HITRAN

GEISA

ExoMars

Line-list

## ABSTRACT

The ExoMars Trace Gas Orbiter (TGO) began its nominal science phase at Mars in April 2018, following releases of editions to two major spectroscopic line lists: GEISA 2015 (Gestion et Etude des Informations Spectroscopiques Atmosphériques: Management and Study of Atmospheric Spectroscopic Information), and HITRAN 2016 (High Resolution Transmission). This work evaluates both line lists over the spectral region between 2325–4350  $\text{cm}^{-1}$  using terrestrial solar occultation observations made by the Atmospheric Chemistry Experiment Fourier Transform Spectrometer (ACE-FTS). This spectral region is targeted on Mars by two complementary solar occultation instruments on TGO that will monitor temperature and pressure, aerosols, the abundance of  $\text{CO}_2$ ,  $\text{CO}$ ,  $\text{H}_2\text{O}$ ,  $\text{HDO}$ ,  $\text{CH}_4$ , and other undetected trace gases. Major updates to GEISA 2015 and HITRAN 2016, with respect to previous editions, have been focused on  $\text{CO}_2$  absorption features in support of Earth-observing missions to monitor greenhouse. Since  $\text{CO}_2$  is the dominant absorber on Mars, making up 96.5% of the atmosphere, validating the updated line lists is critically important before their deployment for ExoMars. We report that updated  $\text{CO}_2$  parameters make significant improvements to spectral fits made when using both line lists. Several updates to  $\text{H}_2\text{O}$  lines in both line lists also show improvement. The primary difference we observe between the two line lists comes from  $\text{O}_3$  absorption features near 3850  $\text{cm}^{-1}$  and from several  $\text{CH}_4$  absorption lines in the regions 2800–3200  $\text{cm}^{-1}$  and 4000–4300  $\text{cm}^{-1}$ . Because of these differences, we find that using HITRAN 2016 tends to result in better spectral fits, especially below 30 km, than using GEISA 2015 in this spectral region. Differences are strongly reduced with increasing altitude ( $> 40$  km) as pressure and gas abundance falls off. It was also discovered that several new errors in both new editions of GEISA and HITRAN were introduced since the HITRAN 2012.

© 2019 Elsevier Ltd. All rights reserved.

## 1. Introduction

New editions of two major spectroscopic line lists have been recently released: Gestion et Etude des Informations Spectroscopiques Atmosphériques: Management and Study of Atmospheric Spectroscopic Information (GEISA) in 2015 [30]; and High Resolution Transmission (HITRAN) in 2016 [26]. Here, we present a comparison of spectral fits to solar occultation measurements of the

Earth's atmosphere made by the Canadian Space Agency's (CSA's) Atmospheric Chemistry Experiment (ACE) Fourier transform spectrometer (FTS) using both line lists. This work was motivated by the arrival of the European Space Agency (ESA) and Roscosmos' ExoMars Trace Gas Orbiter (TGO) at Mars in October 2016. The TGO carries two infrared remote sensing instrument suites, the Atmospheric Chemistry Suite (ACS) [33] and the Nadir and Occultation for Mars Discovery (NOMAD) [65]. Both instrument suites carry channels dedicated to making solar occultation observations at Mars in the infrared wavenumber range of 2325–4350  $\text{cm}^{-1}$ .

The controversial observation of methane ( $\text{CH}_4$ ) in the Martian atmosphere [23,25,36,46,68,69] is one of the key motivations of the ExoMars mission [33,66,74]. NOMAD and ACS will search for  $\text{CH}_4$  by making solar occultation observations of its  $\nu_2$

\* Corresponding author.

E-mail addresses: [kevin.olsen@latmos.ipsl.fr](mailto:kevin.olsen@latmos.ipsl.fr) (K.S. Olsen), [cboone@scisat.ca](mailto:cboone@scisat.ca) (C.D. Boone), [geoffrey.c.toon@jpl.nasa.gov](mailto:geoffrey.c.toon@jpl.nasa.gov) (G.C. Toon), [franck.montmessin@latmos.ipsl.fr](mailto:franck.montmessin@latmos.ipsl.fr) (F. Montmessin), [fedorova@iki.rssi.ru](mailto:fedorova@iki.rssi.ru) (A.A. Fedorova), [korab@iki.rssi.ru](mailto:korab@iki.rssi.ru) (O. Korablev), [trokh@iki.rssi.ru](mailto:trokh@iki.rssi.ru) (A. Trokhimovskiy).

vibration-rotation band centred near  $3000\text{ cm}^{-1}$ , which hosts the strongest absorption features available to both instruments. A key benefit of searching for  $\text{CH}_4$  in this region is that it is relatively clear of interfering absorption lines from  $\text{CO}_2$ . There is a recently-observed, weak vibration-rotation band of carbon dioxide ( $\text{CO}_2$ ) that overlaps  $\text{CH}_4$  in this region [9,67] and one of our specific objectives was to evaluate its spectroscopic parameters in GEISA 2015 and HITRAN 2016.

ACS and NOMAD will also make detailed measurements of water vapour ( $\text{H}_2\text{O}$ ), having the capability of distinguishing isotopologues. The ratio of HDO to  $\text{H}_2\text{O}$  has been used as a critical indicator of the Martian climate in the ancient past [e.g., 22, 35]. The relative abundance of HDO on Mars is enriched relative to Earth, which supports mechanisms for hydrogen escape from the atmosphere, which are preferential towards the lighter isotope [14]. ACS and NOMAD will be able measure the vertical structure of  $\text{H}_2\text{O}$  isotopologues, and monitor their ratios seasonally, spatially, and vertically.

In support of the study of Earth's contemporary climate, and the carbon cycle, with the Orbiting Carbon Observatory (OCO-2) [18,19], the Greenhouse gases Observing SATellite (GOSAT) [72], and the Total Carbon Column Observing Network (TCCON) [71], a large effort has been undertaken to refine and reduce the uncertainty of the spectroscopic parameters of  $\text{CO}_2$ . While the surface pressure of Mars is only between  $550\text{--}720\text{ Pa}$ , roughly  $0.5\text{--}0.7\%$  of Earth's, the volume mixing ratio of  $\text{CO}_2$  is  $0.965$ , or  $2400$  times that on Earth ( $400\text{ ppmv}$ ). Therefore,  $\text{CO}_2$  absorption lines in Mars solar occultation spectra will be deeper and broader than for spectra recorded at Earth, and small changes in the spectroscopic parameters may have a large impact on trace gas retrievals made at Mars.

Our goal was to evaluate the new  $\text{CO}_2$ ,  $\text{H}_2\text{O}$ , and  $\text{CH}_4$  parameters by looking at whether their impact when fitting terrestrial spectra was positive or negative. We have performed spectral fitting for 125 sets of ACE-FTS occultation spectra (resolution of  $0.02\text{ cm}^{-1}$ ) over 50 spectral windows covering the spectral range of  $2430\text{--}4450\text{ cm}^{-1}$  using the HITRAN 2012, HITRAN 2016, and GEISA 2015 line lists.

HITRAN 2016 and GEISA 2015 are compilations of data sources, many of which are shared. One of our most important results is that the updated  $\text{CO}_2$  parameters for some of the stronger vibration-rotation bands, especially those centred at  $3550\text{ cm}^{-1}$  result in strongly improved spectral fits when using either HITRAN 2016 or GEISA 2015. However, we have also found that there are large differences in the spectroscopic parameters of ozone ( $\text{O}_3$ ),  $\text{CH}_4$ , and  $\text{H}_2\text{O}$  between the two data sets, and that using HITRAN 2016 leads to improved spectral fits compared to GEISA 2015. This result is significant since methane is one of the strongest absorbers in the Earth's atmosphere, and is one of the most variable gases. Methane is of key importance for TGO, as ACS and NOMAD both aspire to make its irregular and controversial detection in the Martian atmosphere definitive. However, at this time no methane features have been observed at Mars by TGO instruments [34].

While individual contributions to the line lists are validated, they are often done in laboratory settings, observing controlled gas samples, rather than with observations of an atmosphere [e.g., 26, 30, and references therein]. [3] previously made a direct comparison between  $\text{H}_2\text{O}$  transitions in older versions of GEISA and HITRAN, and qualitatively showed their differences using modelled spectra for Venus at high temperatures and above  $4000\text{ cm}^{-1}$ . A comprehensive validation of the GEISA line list was done using TCCON and the Infrared Atmospheric Sounding Interferometer (IASI) [15] by Armante et al. [1]. They describe a technique used to determine whether spectroscopic parameters should be used to update the GEISA database based on comparisons of computed spectra to observations. They specifically show  $\text{H}_2\text{O}$  and HDO in the ExoMars

region of interest and highlight improvements since GEISA 2011. They also compare  $\text{CH}_4$  lines above  $6000\text{ cm}^{-1}$  to HITRAN 2012 and note an improvement to the residuals. This method was used in the compilation of GEISA 2015 [30].

A comprehensive validation of the HITRAN 2012 line list was undertaken by Toon et al. [60] using the MkIV balloon-borne FTS [59]. They divided the spectral region between  $670\text{--}5620\text{ cm}^{-1}$  into fitting windows and quantitatively evaluated the best-fit residuals across the spectral range and with altitude for several versions of HITRAN released since 2000. They noted specific errors in the data base, where improvements were made, and where previous versions performed better. Their work was influential on the compilation of the latest version of HITRAN evaluated here [26]. Updates to [60] are included in [58] and include evaluation of HITRAN 2016 and the TCCON internal line list, validation with laboratory spectra, and a specific analysis of  $\text{CO}_2$  features. This work follows [60] by using a similar quantitative evaluation technique and covering part of the same spectral region.

## 2. HITRAN 2016

The HITRAN (high-resolution transmission molecular absorption) database was first compiled for the Air Force Geophysics Laboratory (AFGL) by McClatchey et al. [44] and major updated editions have been released on a four year cycle since 1992 [51]. The 2016 version of the HITRAN database [26] describes changes made since the 2012 edition [52]. Among the most significant additions to the database have been the inclusion of spectroscopic parameters for collision-induced broadening from non-nitrogen based atmospheres and for non-Voigt line profiles [70]. The need for line broadening parameters in atmospheres primarily composed of gases other than  $\text{N}_2$  has been motivated by extra-terrestrial spectroscopic applications, e.g., Mars, which is  $96\%$   $\text{CO}_2$ . HITRAN 2016 includes a sparse set of broadening parameters for atmospheres composed of  $\text{H}_2$ , He, or  $\text{CO}_2$  for a subset of gases that includes CO, OCS,  $\text{SO}_2$ ,  $\text{NH}_3$ , HF and HCl, which are all sought at Mars by the ExoMars TGO. For very high-resolution applications, HITRAN 2016 also includes parameters for the speed-dependent Voigt, Galatry, and Hartman-Tran line shapes. These are again only available for a subset of wavenumbers and only for  $\text{H}_2\text{O}$ , CO,  $\text{H}_2$ ,  $\text{O}_2$ ,  $\text{N}_2\text{O}$ , HF and HCl. Because of the complexity of the newly included parameters, newly-developed online tools are now used to create user-defined database versions. The 2016 version also expands the list of available molecules with the addition of  $\text{C}_2\text{N}_2$  and  $\text{COCl}_2$ . While the number of additional lines, and the number of lines for which more accurate measurements have been made, is vast, we will primarily focus on key species relevant to Earth and Mars:  $\text{CO}_2$ ,  $\text{H}_2\text{O}$  and  $\text{CH}_4$ .

For  $\text{CO}_2$ , [26] identifies the imperative for high-accuracy spectroscopic parameters driven by GOSAT, OCO-2, TCCON, and others, and identifies validated improvements between the 2008 and 2012 versions of the HITRAN database [60]. The 2012 version of the database was largely built on theoretical fits of the effective Hamiltonian or effective dipole moments, compiled as the CDSD-296 database [56], supplemented by higher-accuracy experimental measurements made by Toth et al. [61–63]. The line intensity calculations in CDSD-296 have high uncertainties ( $\sim 20\%$ ) and two new sets of theoretical computation have been produced: the Ames list [27] and the UCL-IAO list [73]. These have been extensively validated experimentally, and [26] refers to 14 such studies that show that the UCL-IAO list tends to be more accurate, and that the uncertainties for the 2016 version of HITRAN can be pushed down to the order of  $0.5\%$ . However, the majority of the experimental work focuses on important  $\text{CO}_2$  bands for Earth observation (e.g., for OCO-2) that lie outside the range of high-resolution solar occultation experiments on TGO, above  $5000\text{ cm}^{-1}$  (near  $1.6$

and 2  $\mu\text{m}$ ). Only laboratory measurements presented in [43] and [21] cover the 2300–4400  $\text{cm}^{-1}$  range, and the latter only does so near 3730  $\text{cm}^{-1}$ . The 2016 HITRAN line list for  $\text{CO}_2$  between 2300–4400  $\text{cm}^{-1}$  is a combination of CDS-296 theoretical calculations [56], UCL-IAO or Ames theoretical calculations where better or newly available [27,73], and laboratory measurements where available and with low enough uncertainty [e.g., 21, 43, 63].

For  $\text{H}_2\text{O}$ , the HITRAN 2012 line list was made up of *ab initio* calculations that comprised the BT2 line list [7], with updates, where available, from calculations using a more accurate method [39,40]. Newer calculations using the methodology of [39] have been made as part of an effort by the International Union of Pure and Applied Chemistry (IUPAC) task group [57, and references therein]. The new calculations have been validated experimentally by Birk et al. [10] and the results have been used to update both the IUPAC database and the HITRAN line list. Extensive laboratory measurements have also been made for the German Aerospace Agency (DLR) in the spectral range between 1850–4000  $\text{cm}^{-1}$  by Loos et al. [41,42]. When available, these replace the calculated line strengths of IUPAC and [39].

The  $\text{CH}_4$  data in HITRAN 2012 was comprised of the data set described in [12], which was a combination of theoretical calculations and experimental measurements. This data set replaced over 70% of the HITRAN 2008 line list for  $\text{CH}_4$  [53]. However, analysis of high-resolution solar occultation measurements in the Earth's atmosphere made by the MkIV interferometer [59] determined that there were still several errors and omissions in the HITRAN 2012  $\text{CH}_4$  data [60], especially in the spectral region of the  $\nu_2$  transition critical to ExoMars, near 3000  $\text{cm}^{-1}$ . Errors that were identified were replaced by either the HITRAN 2008 values, or computations made by [64]. Several laboratory studies have been recently undertaken, but the results have not yet been incorporated into the HITRAN line list, but an update to the 2016 edition is expected in the interim [26].

### 3. GEISA 2015

The GEISA line list was first compiled in the early 1970s at the Laboratoire de Météorologie Dynamique (LMD) to support their radiative transfer investigations [13]. Key motivations for the compilation were to include new gases important for planetary atmospheric applications, and to co-develop software tools to easily use the database. One distinguishing feature is to treat certain isotopologues with distinct symmetries as independent species (such as HDO for  $\text{H}_2\text{O}$  and  $\text{CH}_3\text{D}$  for  $\text{CH}_4$ ) [30]. Comparing the available gases in current versions of GEISA and HITRAN,  $\text{GeH}_4$ ,  $\text{C}_3\text{H}_8$ ,  $\text{C}_3\text{H}_4$ , and  $\text{C}_6\text{H}_6$  are unique to GEISA, while  $\text{HOBr}$ ,  $\text{O}$ ,  $\text{H}_2$ , and  $\text{CS}$  are unique to HITRAN. There are also several minor isotopologues of trace gases unique to both. Updates to GEISA are made after evaluating the relevance of new data, the efficiency of including it, and after undergoing a validation process as described in [1].

For  $\text{CO}_2$ , the GEISA 2011 database was replaced by the CDS-296 database [56]. CDS-296 is also the primary source of  $\text{CO}_2$  parameters in the 2016 edition of HITRAN. GEISA also contains three isotopologues not contained in CDS-296 from laboratory measurements by Jacquemart et al. [29,43] (and others at higher wavenumbers than 4400  $\text{cm}^{-1}$ ).

Extensive updates to  $\text{H}_2\text{O}$  were made empirically for GEISA 2015 by a consortium of eight laboratories, nearly tripling the number of available lines since the 2011 edition. In the spectral region of interest to ExoMars ( $\sim 2300$ – $4400$   $\text{cm}^{-1}$ ), these measurements were made by the Laboratoire Inter-Universitaire des Systèmes Atmosphériques (LISA), the Institute of Atmospheric Optics (IAO), and University College, London [30]. Updates to  $\text{H}_2^{16}\text{O}$  come from Coudert et al. [17], and updates for  $\text{H}_2^{17}\text{O}$  and  $\text{H}_2^{18}\text{O}$  come from

Lodi et al. [39,40] and the IUPAC efforts, which is the same source as for HITRAN 2016. These were supplemented or updated by measurements made by [16]. GEISA 2015 also newly includes lines for two isotopologues of  $\text{D}_2\text{O}$  not included in HITRAN.

Updates to  $\text{CH}_4$  in this spectral range mainly come from the work of [47,48] which use the same methodology as [12] (HITRAN 2012). The validation work of [1] showed some imprecision in the new parameters, resulting in some  $\text{CH}_4$  lines from GEISA 2011 being retained.

### 4. Methodology

In this study, we break the wavenumber range of the ExoMars solar occultation spectrometers up into discrete fitting windows and analyze terrestrial solar occultation spectra recorded by ACE-FTS using the Jet Propulsion Laboratory Gas Fitting (GFIT or GGG) software suite. 125 occultations were analyzed. During an occultation, a series of observations of the sun are made while the limb of the atmosphere lies between the solar disk and the instrument. For each window, residuals were computed for each altitude level. The means of the residuals were taken at levels of equal pressure, and the root-mean-square (RMS) and standard deviation ( $\sigma$ ) were computed for each fitting window. The means of the residuals were taken, rather than computing the residuals of mean spectra, due to variations in line depths between occultations, especially for  $\text{CH}_4$  lines. In general, the lower the results RMS of the mean residuals is, the more accurate the spectroscopic parameters used in the fitting are. This methodology is very similar to that used by Toon et al. [60] who analyzed MkIV spectra.

ACE-FTS is a compact, double-pass interferometer with a spectral resolution of 0.02  $\text{cm}^{-1}$  and a spectral range of 750–4400  $\text{cm}^{-1}$ . It has been operating continuously in low-Earth orbit since 2003. The 125 ACE-FTS occultations analyzed were recorded between 2004 and 2012 and are unrestricted in longitude and season. Most observations are at high latitudes due to the ACE orbit (650 km with an inclination of 74°). A sequence of measurements is made with an observation every 1–6.5 km, and on average every 4 km. Two detectors provide an simultaneous spectral range of 750–4400  $\text{cm}^{-1}$  [8].

Spectral fitting in this study was done with GGG, which is also being used to analyze solar occultation observations made by ACS on ExoMars. GGG is developed from early Occultation Display Spectra (ODS) used by the ATMOS FTS that flew on the space shuttle [28,49]. It is a robust software suite adaptable for solar occultations [50,59,60], ground based observations [71], or laboratory measurements. For each altitude and each fitting window, GGG computes a spectrum from a set of parameters that include the calculated optical path, vertical profiles of pressure and temperature, and *a priori* gas volume mixing ratio (VMR) vertical profiles. GGG then performs non-linear least squares fitting to adjust VMR scaling factors (as well as other optional parameters such as continuum level and frequency shift) to obtain a best fit. Retrieved VMR vertical profiles can be obtained by inverting the matrix of VMR scale factors for each target gas at each altitude, with the matrix of slant paths [54,71].

*A priori* temperature, pressure, and specific humidity vertical profiles were derived from National Centers for Environmental Prediction (NCEP) reanalysis data [32] up to 40 km. The US standard atmosphere was used above 40 km.

For this work, we consider the fitting residuals for each window and focus on three pressure levels where we take the means of the residuals: 0.052, 0.0029, and 0.00023 atm, corresponding to 20, 40, and 60 km respectively. For each occultation, fitting was performed at all altitudes and in all spectral windows. The closest altitude level to the predetermined pressure levels was identified.

**Table 1**

List of spectral fitting windows used to evaluate the HITRAN 2016 and GEISA 2015 line lists with ACE-FTS solar occultation observations of the Earth's atmosphere. Given for each fitting window are: centre wavenumber, window width, and gases fit in the window.

Centre $\bar{\nu}$ ( $\text{cm}^{-1}$ )	Width ( $\text{cm}^{-1}$ )	Gases fit
2455.5	25.9	CO <sub>2</sub> , CH <sub>4</sub> , H <sub>2</sub> O, N <sub>2</sub> O, O <sub>3</sub>
2491.5	47.9	CO <sub>2</sub> , CH <sub>4</sub> , H <sub>2</sub> O, N <sub>2</sub> O, O <sub>3</sub>
2551.55	71.35	H <sub>2</sub> O, CO <sub>2</sub> , O <sub>3</sub> , N <sub>2</sub> O, CH <sub>4</sub>
2615.74	56.2	CO <sub>2</sub> , CH <sub>4</sub> , H <sub>2</sub> O, N <sub>2</sub> O, O <sub>3</sub> , HCl, C <sub>2</sub> H <sub>6</sub>
2666.6	44.76	H <sub>2</sub> O, CO <sub>2</sub> , O <sub>3</sub> , N <sub>2</sub> O, CH <sub>4</sub> , HCl, C <sub>2</sub> H <sub>6</sub>
2689.8	0.62	HDO, CO <sub>2</sub> , O <sub>3</sub> , N <sub>2</sub> O, CH <sub>4</sub>
2692.76	0.55	HDO, CO <sub>2</sub> , O <sub>3</sub> , N <sub>2</sub> O, CH <sub>4</sub>
2708.17	0.54	HDO, CO <sub>2</sub> , O <sub>3</sub> , N <sub>2</sub> O, CH <sub>4</sub>
2722.25	52.0	CO <sub>2</sub> , CH <sub>4</sub> , C <sub>2</sub> H <sub>6</sub> , H <sub>2</sub> O, N <sub>2</sub> O, O <sub>3</sub> , HCl, HDO
2780.74	65.15	CO <sub>2</sub> , CH <sub>4</sub> , C <sub>2</sub> H <sub>6</sub> , H <sub>2</sub> O, N <sub>2</sub> O, O <sub>3</sub> , HCl, HDO
2801.6	0.49	HDO, CO <sub>2</sub> , O <sub>3</sub> , N <sub>2</sub> O, CH <sub>4</sub>
2825.0	22.95	H <sub>2</sub> O, O <sub>3</sub> , N <sub>2</sub> O, CH <sub>4</sub> , HDO, HCl
2849.15	24.55	HDO, CO <sub>2</sub> , H <sub>2</sub> O, CH <sub>4</sub> , C <sub>2</sub> H <sub>6</sub> , O <sub>3</sub> , N <sub>2</sub> O, HCl
2904.43	85.10	H <sub>2</sub> O, O <sub>3</sub> , N <sub>2</sub> O, CH <sub>4</sub> , HDO, HCl, NO <sub>2</sub> , OCS
2973.65	1.21	C <sub>2</sub> H <sub>6</sub> , CO <sub>2</sub> , H <sub>2</sub> O, CH <sub>4</sub> , O <sub>3</sub>
2978.2	62.0	CO <sub>2</sub> , CH <sub>4</sub> , C <sub>2</sub> H <sub>6</sub> , C <sub>2</sub> H <sub>4</sub> , H <sub>2</sub> O, O <sub>3</sub> , HCl, HDO
2983.49	0.78	C <sub>2</sub> H <sub>6</sub> , CO <sub>2</sub> , O <sub>3</sub> , CH <sub>4</sub>
2986.74	0.58	C <sub>2</sub> H <sub>6</sub> , CO <sub>2</sub> , O <sub>3</sub>
2989.98	0.80	C <sub>2</sub> H <sub>6</sub> , CO <sub>2</sub> , O <sub>3</sub> , CH <sub>4</sub>
2993.52	1.23	C <sub>2</sub> H <sub>6</sub> , CO <sub>2</sub> , O <sub>3</sub> , CH <sub>4</sub> , H <sub>2</sub> O
3022.13	18.14	CH <sub>4</sub> , H <sub>2</sub> O, C <sub>2</sub> H <sub>6</sub> , C <sub>2</sub> H <sub>4</sub> , O <sub>3</sub> , HCl
3035.08	9.2	CH <sub>4</sub> , H <sub>2</sub> O, C <sub>2</sub> H <sub>6</sub> , C <sub>2</sub> H <sub>4</sub> , O <sub>3</sub>
3057.72	5.1	CH <sub>4</sub> , H <sub>2</sub> O, O <sub>3</sub>
3065.86	3.35	CH <sub>4</sub> , H <sub>2</sub> O, O <sub>3</sub>
3077.36	2.54	CH <sub>4</sub> , H <sub>2</sub> O, O <sub>3</sub>

**Table 2**

List of spectral fitting windows used to evaluate the HITRAN 2016 and GEISA 2015 line lists with ACE-FTS solar occultation observations of the Earth's atmosphere. Given for each fitting window are: centre wavenumber, window width, and gases fit in the window.

Centre $\bar{\nu}$ ( $\text{cm}^{-1}$ )	Width ( $\text{cm}^{-1}$ )	Gases fit
3089.75	17.5	CH <sub>4</sub> , H <sub>2</sub> O, C <sub>2</sub> H <sub>6</sub> , C <sub>2</sub> H <sub>4</sub> , CO <sub>2</sub> , O <sub>3</sub>
3126.65	58.0	CO <sub>2</sub> , CH <sub>4</sub> , C <sub>2</sub> H <sub>4</sub> , H <sub>2</sub> O, O <sub>3</sub> , HDO
3202.0	90.0	H <sub>2</sub> O, CO <sub>2</sub> , CH <sub>4</sub> , O <sub>3</sub> , HCN
3292.0	90.0	H <sub>2</sub> O, CO <sub>2</sub> , CH <sub>4</sub> , O <sub>3</sub> , HCN, N <sub>2</sub> O
3391.15	108.6	CO <sub>2</sub> , H <sub>2</sub> O, C <sub>2</sub> H <sub>2</sub> , NH <sub>3</sub> , HCN, N <sub>2</sub> O, O <sub>3</sub> , HDO
3489.0	86.0	H <sub>2</sub> O, CO <sub>2</sub> , O <sub>3</sub> , N <sub>2</sub> O
3577.0	86.0	H <sub>2</sub> O, CO <sub>2</sub> , O <sub>3</sub> , N <sub>2</sub> O, HNO <sub>3</sub> , HDO
3665.0	86.0	H <sub>2</sub> O, CO <sub>2</sub> , O <sub>3</sub> , N <sub>2</sub> O, HNO <sub>3</sub> , HDO
3753.0	86.0	H <sub>2</sub> O, CO <sub>2</sub> , O <sub>3</sub> , N <sub>2</sub> O, HF, HDO
3798.8	7.46	H <sub>2</sub> O, CO <sub>2</sub> , CH <sub>4</sub> , O <sub>3</sub>
3822.5	51.0	CO <sub>2</sub> , H <sub>2</sub> O, N <sub>2</sub> O, O <sub>3</sub> , CH <sub>4</sub> , HF, HDO
3869.14	42.0	H <sub>2</sub> O, CO <sub>2</sub> , O <sub>3</sub> , N <sub>2</sub> O, CH <sub>4</sub> , HF, HDO
3895.36	10.18	H <sub>2</sub> O, CO <sub>2</sub> , CH <sub>4</sub> , O <sub>3</sub>
3903.93	6.17	H <sub>2</sub> O, CO <sub>2</sub> , CH <sub>4</sub> , O <sub>3</sub>
3936.15	58.0	CO <sub>2</sub> , H <sub>2</sub> O, N <sub>2</sub> O, O <sub>3</sub> , CH <sub>4</sub> , HF, HDO
3967.79	2.0	H <sub>2</sub> O, CO <sub>2</sub> , CH <sub>4</sub> , O <sub>3</sub>
4026.0	114.0	H <sub>2</sub> O, CO <sub>2</sub> , O <sub>3</sub> , N <sub>2</sub> O, CH <sub>4</sub> , HF, CO
4085.69	3.4	HDO, CO, H <sub>2</sub> O, O <sub>3</sub> , CH <sub>4</sub>
4115.21	5.62	HDO, CO, O <sub>3</sub> , CH <sub>4</sub>
4128.34	9.53	HDO, CO, H <sub>2</sub> O, O <sub>3</sub> , CH <sub>4</sub>
4132.1	72.5	CO, H <sub>2</sub> O, CO <sub>2</sub> , CH <sub>4</sub> , O <sub>3</sub>
4214.2	94.1	CO, H <sub>2</sub> O, CO <sub>2</sub> , CH <sub>4</sub> , O <sub>3</sub>
4300.4	76.6	CO, H <sub>2</sub> O, CH <sub>4</sub> , O <sub>3</sub>
4377.0	75.4	H <sub>2</sub> O, O <sub>3</sub> , CH <sub>4</sub> , N <sub>2</sub> O, CO
4436.2	42.6	CO <sub>2</sub> , H <sub>2</sub> O, CH <sub>4</sub>

The residuals were computed for each window and the RMS and standard deviation were computed from the residual as:

$$\text{RMS}^2 = \sum x_i^2 / N,$$

$$\sigma^2 = \sum (x_i - \bar{x})^2 / (N - 1), \quad (1)$$

where  $N$  is the number of spectral points,  $x_i$  is the residual value at the  $i$ th spectral point, and  $\bar{x}$  is the mean of the residual. In general, for this application  $\bar{x} \sim 0$  and  $\text{RMS}^2 \sim \sigma^2$ . For strong deviations between the computed and observed spectra,  $\sigma^2$  will reflect the magnitude of deviations from the mean of the residuals, while the RMS will reflect the deviation from zero, which is the expected outcome for a good fit. Therefore, the presented results will use the RMS values.

The fitting windows used are given in Tables 1 and 2, and panel a in Fig. 1 shows their distribution over a sample of ACE-FTS solar occultation transmission spectrum. Panels b–e in Fig. 1 illustrate the locations and magnitudes of absorption features due to major gas species in the Earth's atmosphere: CO<sub>2</sub>, H<sub>2</sub>O, CH<sub>4</sub>, O<sub>3</sub>, and N<sub>2</sub>O.

## 5. Results

We begin with an overview of the differences between the HITRAN 2016 and GEISA 2015 line lists in the ExoMars spectral region of interest, 2325–4350  $\text{cm}^{-1}$ . Fig. 2 shows mean ACE-FTS spectra averaged at three different pressure levels corresponding to approximately 20, 40, and 60 km tangent altitudes. Each primary panel, for each pressure level, shows the mean ACE-FTS spectra, averaged over 125 occultations, for each fitting window (Fig. 2 does not show continuous ACE-FTS spectra). Shown over top of the mean ACE-FTS spectra, is the mean of the calculated best fits for each window when using the HITRAN 2016 line list (as an example). It is important to note that the noise level of the ACE-FTS spectra is not constant with wavenumber [11], and the noise can

be seen increasing towards higher wavenumbers in Fig. 2, even after averaging the ACE-FTS spectra.

The secondary panels in Fig. 2 show the mean residuals for each fitting window at each pressure level. Shown are mean residuals when fitting with HITRAN 2012, GEISA 2015, and HITRAN 2016. HITRAN 2012 tends to have the largest numbers of errors and both newer line lists improve upon it. The most significant errors are in the CO<sub>2</sub> band centred at 3508  $\text{cm}^{-1}$ , which were corrected in the 2016 edition (and not present in GEISA 2015). Difficulty in fitting strong CO<sub>2</sub> lines in the region between 3500–3600  $\text{cm}^{-1}$  persists when using all three line lists, but this is also due to a strong increase in detector noise in that region, visible in the mean spectra, especially at the lowest pressure level.

In general, HITRAN 2016 performs better than GEISA 2015, and larger mean residuals are seen in Fig. 2. The largest differences are observed the lowest pressure levels, while both line lists perform similarly at higher tangent altitudes. This suggests that the errors are related to either increased pressure and pressure broadening at lower altitudes, or (and) that the magnitude of the errors are related to line depth, and that when the line depths are small, the errors are less than the instrument noise. When CH<sub>4</sub> or CO<sub>2</sub> lines are saturated, the residuals show the negative impact of untreated line mixing, which was not implemented in this spectral region for this study, but is available in GGG [45]. Key areas that GEISA 2015 has difficulty with relative to HITRAN 2016 are between 2700–3200  $\text{cm}^{-1}$ , when strong CH<sub>4</sub> lines absorb totally, between 4100–4300  $\text{cm}^{-1}$ , where errors are related to O<sub>3</sub> lines and also CH<sub>4</sub> lines (shown in the following section). These are also errors near 3800  $\text{cm}^{-1}$  related to H<sub>2</sub>O. Fitting the strong CO<sub>2</sub> lines between 3500–3700  $\text{cm}^{-1}$  is challenging for GGG using any line list, as shown in Fig. 2, especially the middle pressure level. The  $\nu_1$  band of HNO<sub>3</sub> is located in this region which is significant at 20 km.

At lower wavenumbers, where detector noise is lowest, there are systematic features observable in the mean residuals when

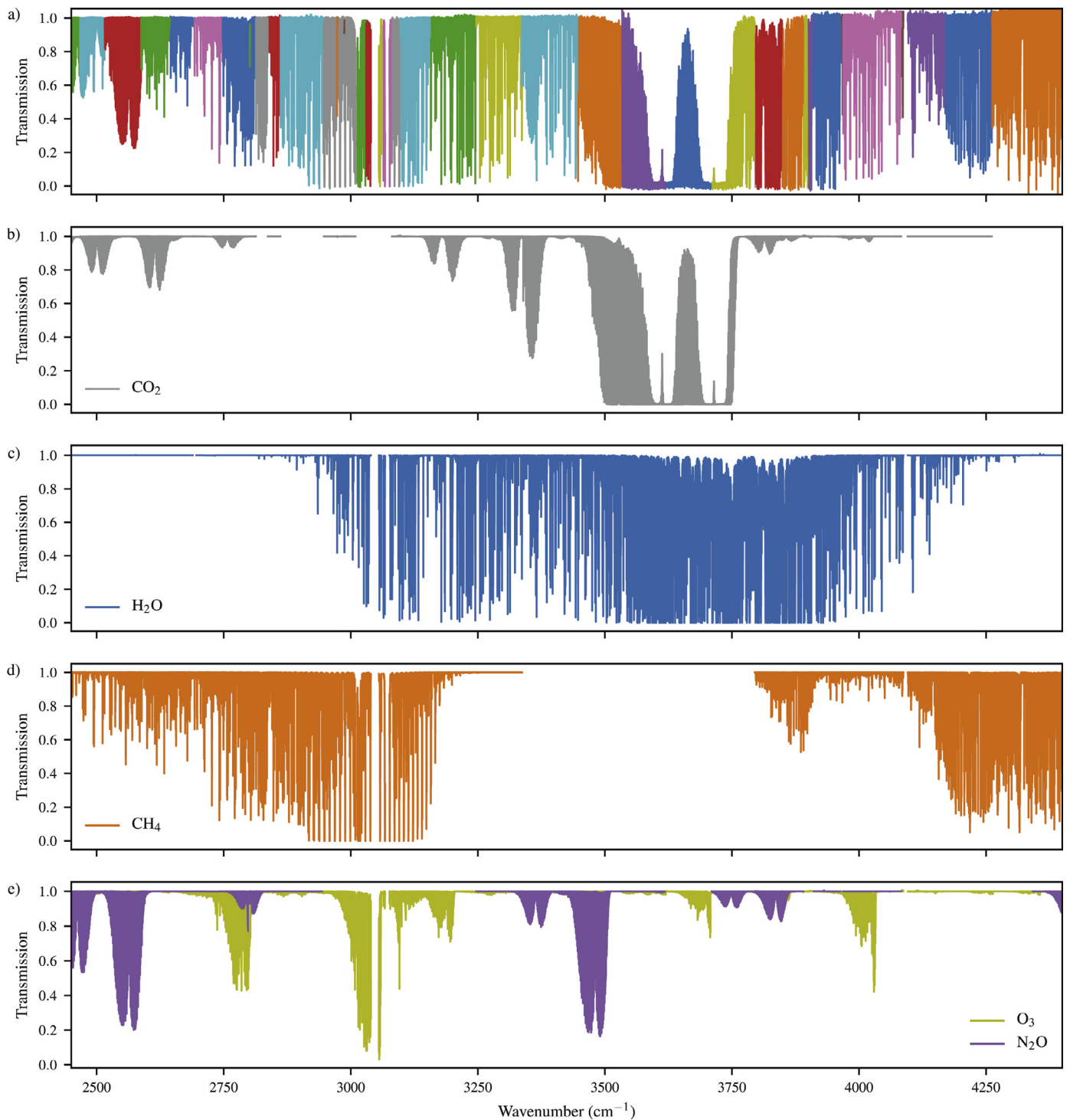


**Fig. 1.** A look at ACE-FTS observations in the ExoMars spectral region of interest: (a) mean ACE-FTS spectra at the 0.052 atm pressure level (near 20 km), the colours indicate different fitting windows; (b) contributions from CO<sub>2</sub>; (c) contributions from H<sub>2</sub>O; (d) contributions from CH<sub>4</sub>; (e) contributions from O<sub>3</sub> and N<sub>2</sub>O.

using either line list. Near 2550 cm<sup>-1</sup>, this is related to line widths in an N<sub>2</sub>O absorption band. Near 2650 cm<sup>-1</sup>, there is an observed absorption band of HNO<sub>3</sub> that is not included in either line list. Several HNO<sub>3</sub> bands are observable in ACE-FTS spectra that are not contained in the HITRAN or GEISA line lists. Weaker bands result in an apparent baseline curvature, while stronger bands show a distinct vibration-rotation band structure in the residuals. Examples are shown in the following section.

Fig. 3 shows the mean RMS for each fitting window, at each pressure level. The RMS was computed for each ACE-FTS occultation in a given window, and shown are the means of the RMS values, with the standard deviation of the mean. At the highest pressure level (top panel, near 60 km), all three line lists perform similarly. In the middle pressure level, near 40 km, we observe strong increases in the mean RMS values, and their uncertainties, where line depths extend beyond 50%, just above 3500 cm<sup>-1</sup> due

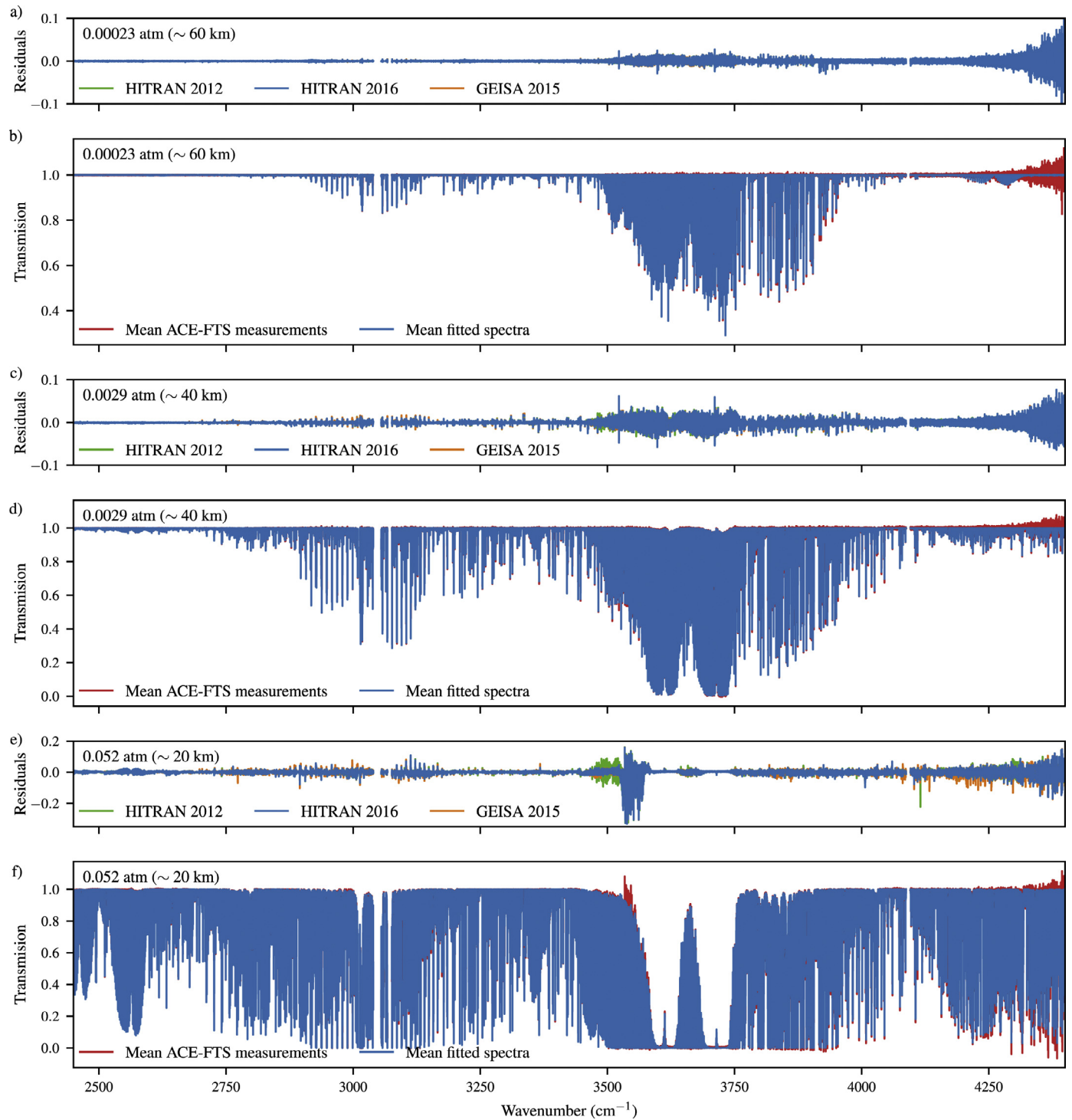


**Fig. 2.** Mean ACE-FTS spectra, mean best-fit computed spectra, and mean residuals for each fitting window. Mean residuals are shown using HITRAN 2012 (green), HITRAN 2016 (blue) and GEISA 2015 (orange). Mean fitted spectra are shown only for when using HITRAN 2016. (a) mean residuals from 0.00023 atm ( $\sim 60$  km), (b) mean spectra and mean fits from 0.00023 atm, (c) mean residuals from 0.0029 atm ( $\sim 40$  km), (d) mean spectra and mean fits from 0.0029 atm, (e) mean residuals from 0.052 atm ( $\sim 20$  km), (f) mean spectra and mean fits from 0.052 atm. (For interpretation of the references to colour in this figure legend, the reader is referred to the web version of this article.)

to CO<sub>2</sub>, and near 3000 cm<sup>-1</sup> due to CH<sub>4</sub>. At the lowest pressure level, the RMS uncertainties increase strongly for all windows, and the differences between line lists become most apparent. At this level, we see deviations between HITRAN 2012 and 2016, at the same locations observed in Fig. 2. This analysis also supports the observations made from Fig. 2 regarding GEISA 2015. Specific examples and windows are explored in the following section.

## 6. Specific examples

### 6.1. 2440 – 2660 cm<sup>-1</sup>: N<sub>2</sub>O and HNO<sub>3</sub>

The spectral region between 2440 – 2660 cm<sup>-1</sup> was covered by four broad fitting windows centred at 2455.5, 2491.5, 2551.55, and 2615.74 cm<sup>-1</sup>. This region is characterized primarily by the *P* and

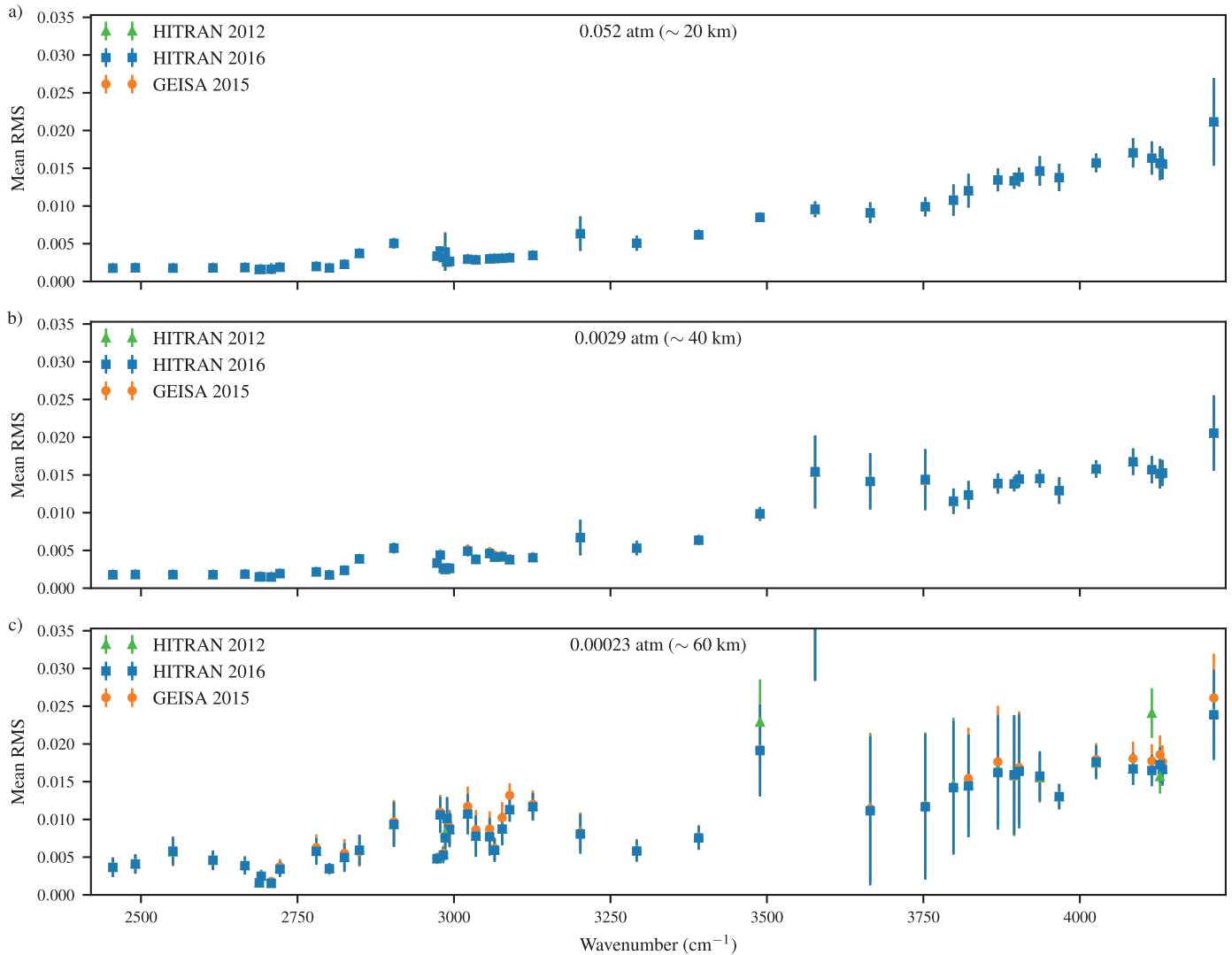


**Fig. 3.** Mean RMS values computes for each fitting window when using each HITRAN 2012, HITRAN 2016, and GEISA 2015 at three pressure levels: (a) 0.00023 atm ( $\sim 60$  km), (b) 0.0029 atm ( $\sim 40$  km), (c) 0.052 atm ( $\sim 20$  km).

$R$  branches of two vibration-rotation bands of  $N_2O$ , centred near  $2462$  and  $2562$   $cm^{-1}$ , and two vibration-rotation bands of  $CO_2$ , centred near  $2501$  and  $2614$   $cm^{-1}$ . For these bands, all three spectroscopic line lists perform similarly. In the  $2491.5$   $cm^{-1}$  window, small, but visible, improvements are apparent where  $CO_2$  lines are present in the two updated editions of the line lists when compared to HITRAN 2012.

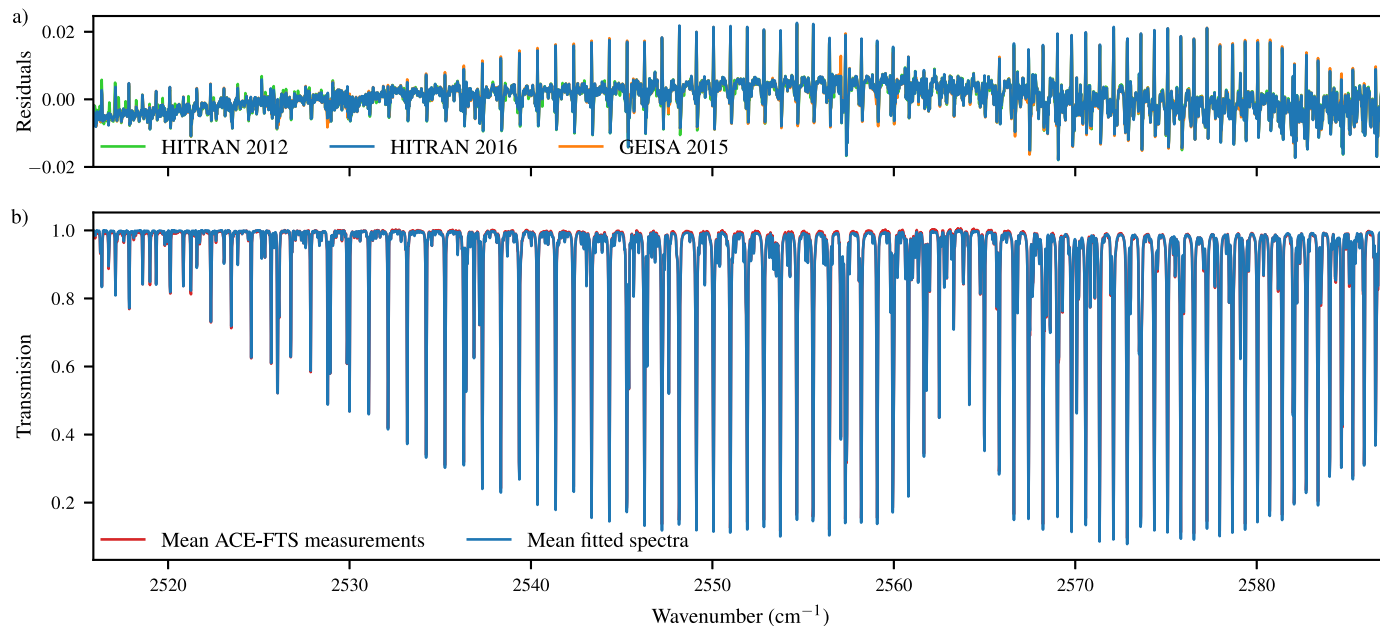
Both the GEISA 2015 and HITRAN 2016 line lists perform almost equivalently in this region. However, there are apparent problems in the fitting, and these problems persist in both data sets. At the lower pressure level, the  $N_2O$  fits produce large mean residuals whose shape is indicative of errors in line width. These errors do not persist at the higher pressure levels and are likely due to errors in the broadening parameters in the line lists. The mean ACE-FTS spectra and mean residuals for the  $2551.55$   $cm^{-1}$  window, which are shown in Fig. 4. The lines in this window are mainly due to  $N_2O$ , with some  $CH_4$  lines throughout, and the edge of an  $R$  branch of  $CO_2$  on the left side.

Fig. 5 shows the same information as Fig. 4, but for the  $2615.74$   $cm^{-1}$  window. Again, both the GEISA 2015 and HITRAN 2016 line lists perform equivalently, and, again, there are systematic differences between the observations and the computed spectra. These differences are due to  $HNO_3$  lines not included in ei-

ther line list. The broad curvature of the baseline in the residuals is due to a weaker band, while the distinct peaks to the right side of Fig. 4 are the  $P$  branch of a stronger  $HNO_3$  vibration-rotation band. There is a corresponding  $R$  branch in the adjacent  $2666.6$   $cm^{-1}$  window. The feature of another weak  $HNO_3$  band is also present in the  $2491.5$   $cm^{-1}$  window, and stronger missing lines are seen in the  $2978.2$   $cm^{-1}$  window, between  $2985$ – $3010$   $cm^{-1}$ , and in the  $3391.15$   $cm^{-1}$  window, between  $3390$ – $3415$   $cm^{-1}$ . That these are due to  $HNO_3$  is verified by measurements made for the line list distributed by the Pacific Northwest National Laboratory (PNNL) [31,55]. Supplementary  $HNO_3$  line lists are used for ACE-FTS and TCCON retrievals.

## 6.2. $2660 - 3440$ $cm^{-1}$ : $CH_4$

This wavenumber region is characterized by strong  $CH_4$  absorption features, but also contains important bands of  $O_3$ ,  $N_2O$  and  $CO_2$ . This region was covered by several narrow windows and 12 wide windows ranging in width between  $18$ – $108$   $cm^{-1}$ . The first window centred at  $2722.25$   $cm^{-1}$  features three strong  $CH_4$  lines, and many associated weaker lines, and there are significant residual errors about each due to unaccounted line mixing. Toon et al. [60] pointed out a positional error in a  $CH_4$  line at



**Fig. 4.** (a) Mean residuals for the 2551.55  $\text{cm}^{-1}$  window at 0.052 atm ( $\sim 20$  km) with HITRAN 2012, HITRAN 2016, and GEISA 2015. (b) Mean measured ACE-FTS spectrum and mean computed spectrum (for HITRAN 2016). The primary features in this window are  $\text{N}_2\text{O}$  lines and the residuals correspond to the  $\text{N}_2\text{O}$  lines.

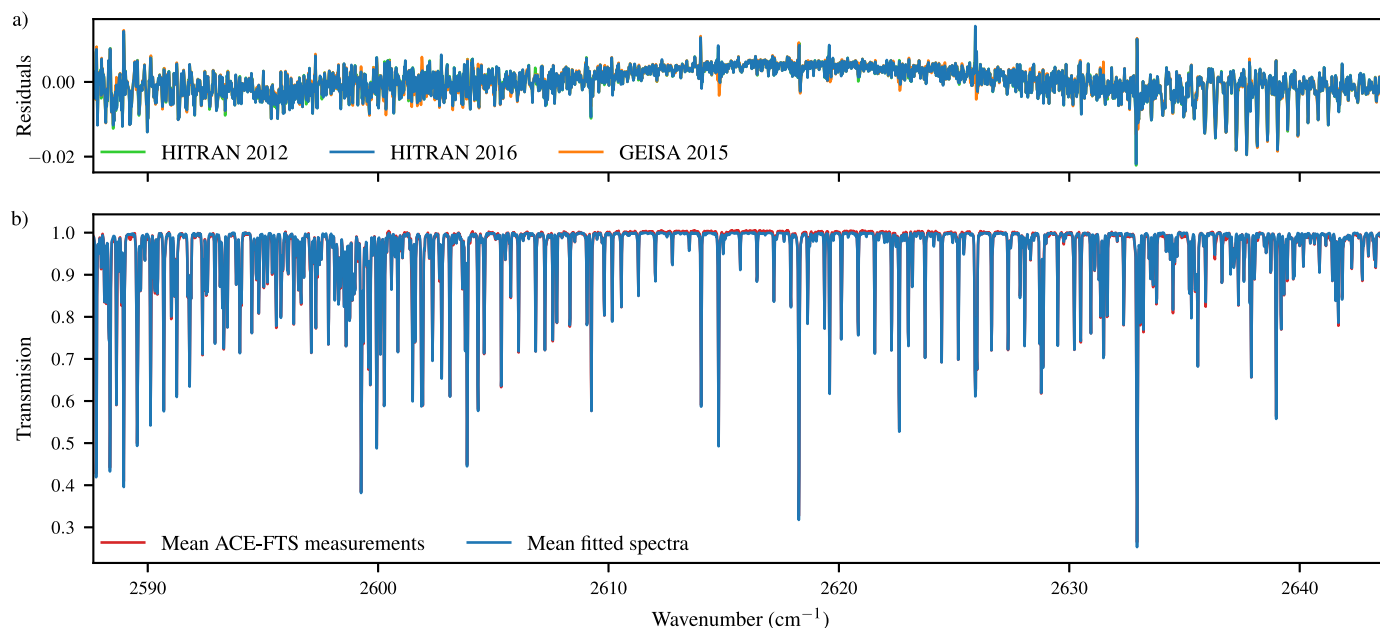


**Fig. 5.** (a) Mean residuals for the 2615.74  $\text{cm}^{-1}$  window at 0.052 atm ( $\sim 20$  km) with HITRAN 2012, HITRAN 2016, and GEISA 2015. (b) Mean measured ACE-FTS spectrum and mean computed spectrum (for HITRAN 2016). The main features are from  $\text{N}_2\text{O}$  towards the left edge, a  $\text{CO}_2$  band across the entire window, and several strong  $\text{CH}_4$  lines. The residuals are due to  $\text{HNO}_3$ .

2742.3  $\text{cm}^{-1}$  that was introduced into HITRAN 2012 after the 2008 version. This error is present in GEISA 2015 and HITRAN 2016, and is shown in Fig. 6a. While positive changes have been made to the HITRAN 2016 line list, correcting the positional error, strong residual features remain, but these are most likely due to unaccounted line mixing for such strong lines fit at a low altitude. This window also features several weak  $\text{O}_3$  lines that are well fit by both line lists, except a small region around 2705–2710  $\text{cm}^{-1}$  where fitting with GEISA 2015 results in larger mean residuals than fitting with HITRAN 2016, on the order of 0.005.

The window centred at 2780.74  $\text{cm}^{-1}$  contains weaker  $\text{CH}_4$  lines and a large  $\text{O}_3$  band. Both line lists perform similarly here, but there is what appears to be a single missing line in the GEISA

2015 list. This is an ozone line at 2773.15  $\text{cm}^{-1}$  that is not missing, but has an error in line strength, shown in Fig. 6b. Toon et al. [60] pointed out an error in position in an  $\text{O}_3$  resonance transition at 2761.42  $\text{cm}^{-1}$  that is seen in HITRAN 2012 and GEISA 2015, but has been corrected in HITRAN 2016. However, there are new  $\text{O}_3$  positional errors at 2763.86 and 2798.0  $\text{cm}^{-1}$  in the HITRAN 2016 line list that were not present in HITRAN 2012.

The fitting window centred at 2825.0  $\text{cm}^{-1}$  presents one of the largest discrepancies between HITRAN 2016 and GEISA 2015. The mean ACE-FTS spectra and mean residuals when fitting with the three line lists are shown in Fig. 7 for the lowest pressure level. These discrepancies are characteristic of the strong  $\text{CH}_4$  lines throughout this region, and the systematic differentiation between

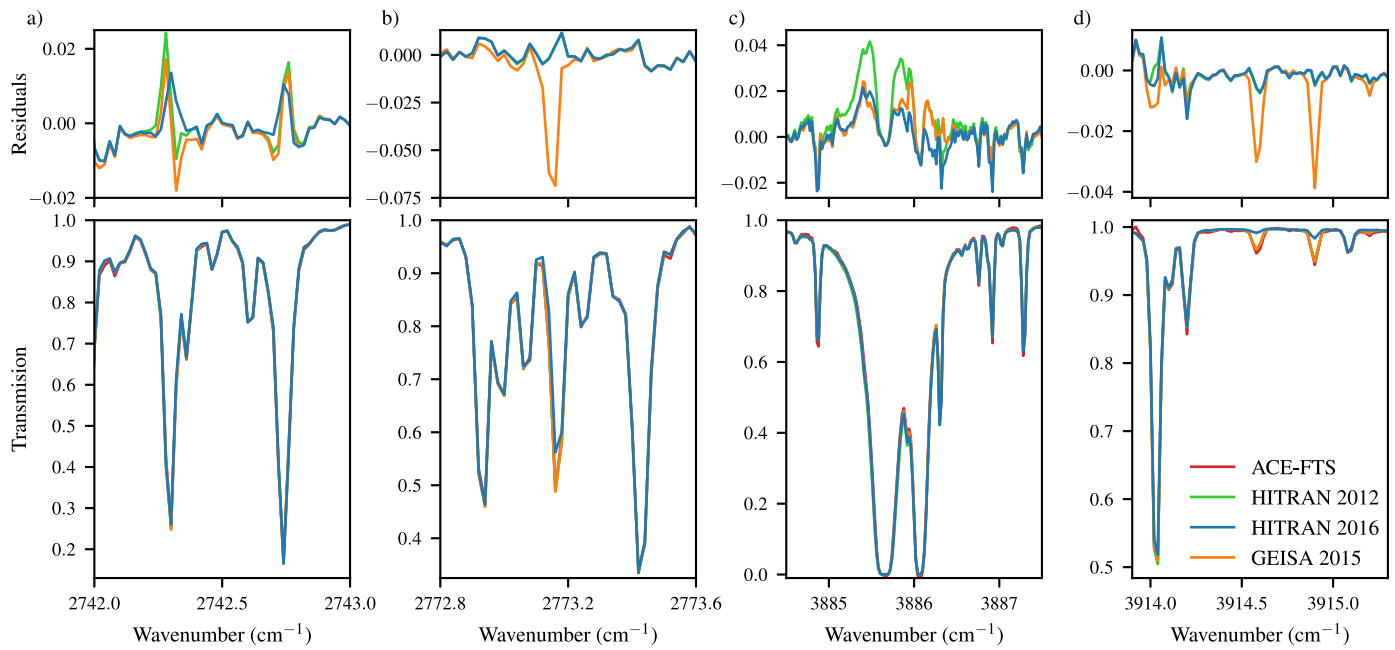


**Fig. 6.** Zoom of the residuals and mean spectra (as in Figs. 4 and 5) where errors are present, for the windows: (a) 2722.25  $\text{cm}^{-1}$ , (b) 2780.74  $\text{cm}^{-1}$ , (c) 3869.14  $\text{cm}^{-1}$ , (d) 3936.15  $\text{cm}^{-1}$ .

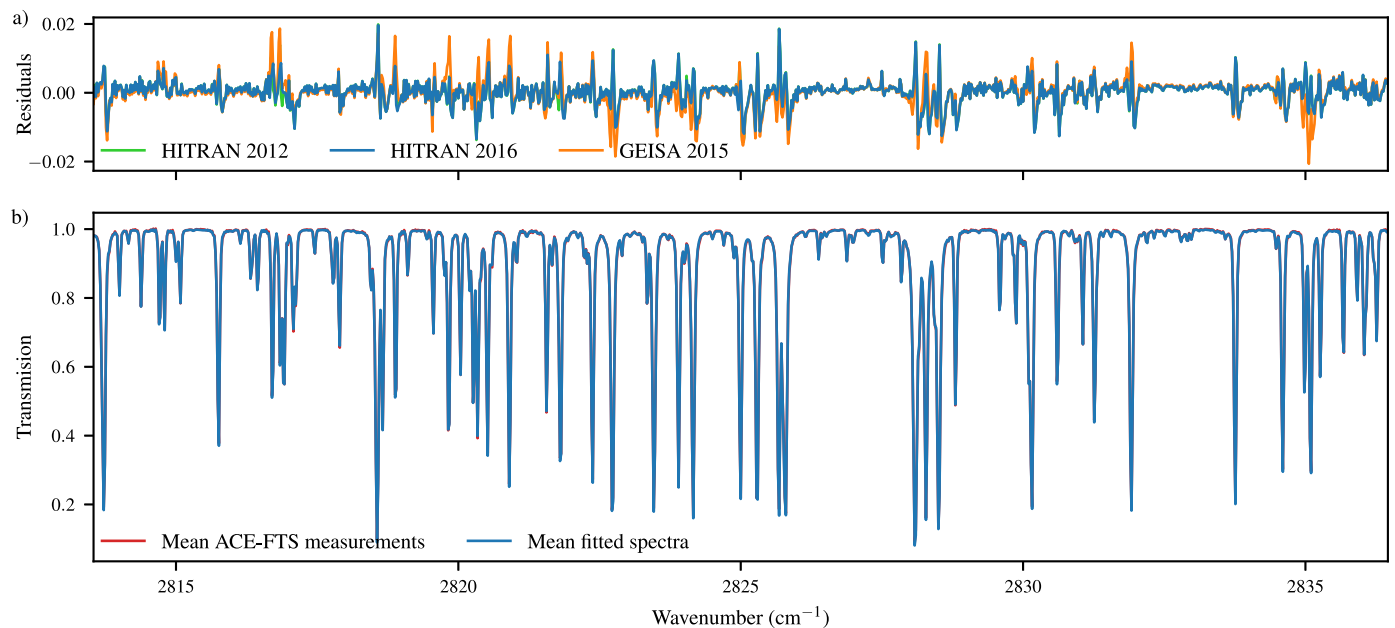


**Fig. 7.** a) Mean residuals for the 2825.0  $\text{cm}^{-1}$  window at 0.052 atm ( $\sim 20$  km) with HITRAN 2012, HITRAN 2016, and GEISA 2015. b) Mean measured ACE-FTS spectrum and mean computed spectrum (for HITRAN 2016). Features are primarily  $\text{CH}_4$  lines.

fitting results using the two line lists is seen in Fig. 3. There is little difference between the two versions of HITRAN, and both result in mean residual errors on the order of  $\pm 0.01$  about strong  $\text{CH}_4$  lines. In several positions, however, when fitting with GEISA 2015, these residuals can be twice as large.

Windows centred at 2849.15, 2904.43, 2978.2, and 3126.65  $\text{cm}^{-1}$  are similar to those preceding, predominantly featuring strong  $\text{CH}_4$  lines, with line mixing errors apparent in the mean residuals when using either line list, but the largest residuals are found when using GEISA 2015. In the 2978.2  $\text{cm}^{-1}$  window, there are several saturated (at low altitude)  $\text{CH}_4$  lines, and the beginning of a broad, strong band of  $\text{O}_3$  lines, but also a set of  $\text{HNO}_3$  lines that are missing in both line lists.

The 3022.13  $\text{cm}^{-1}$  window contains a mixture of strong  $\text{O}_3$  and  $\text{CH}_4$  lines. There is an opaque region about 5  $\text{cm}^{-1}$  wide at the lower pressure level, which is the Q-branch of this  $\text{CH}_4$  band. This feature is critically important for ExoMars, as it is the strongest and broadest  $\text{CH}_4$  feature in the available wavenumber range, and where the ExoMars instruments will focus their search for a  $\text{CH}_4$  signature. Mean residuals on the right side of the Q-branch (3018  $\text{cm}^{-1}$ ) are nearly equivalent when using GEISA 2015 or HITRAN 2016. On the left side (3015  $\text{cm}^{-1}$ ), mean residuals when using GEISA 2015 are larger than when using HITRAN 2016 by 0.01–0.02. Most of the fitting differences in this region can be attributed to  $\text{CH}_4$ , but there is also a weaker  $\text{HCl}$  line at 3014.4  $\text{cm}^{-1}$  that contributes to these differences. Note that the residuals for both

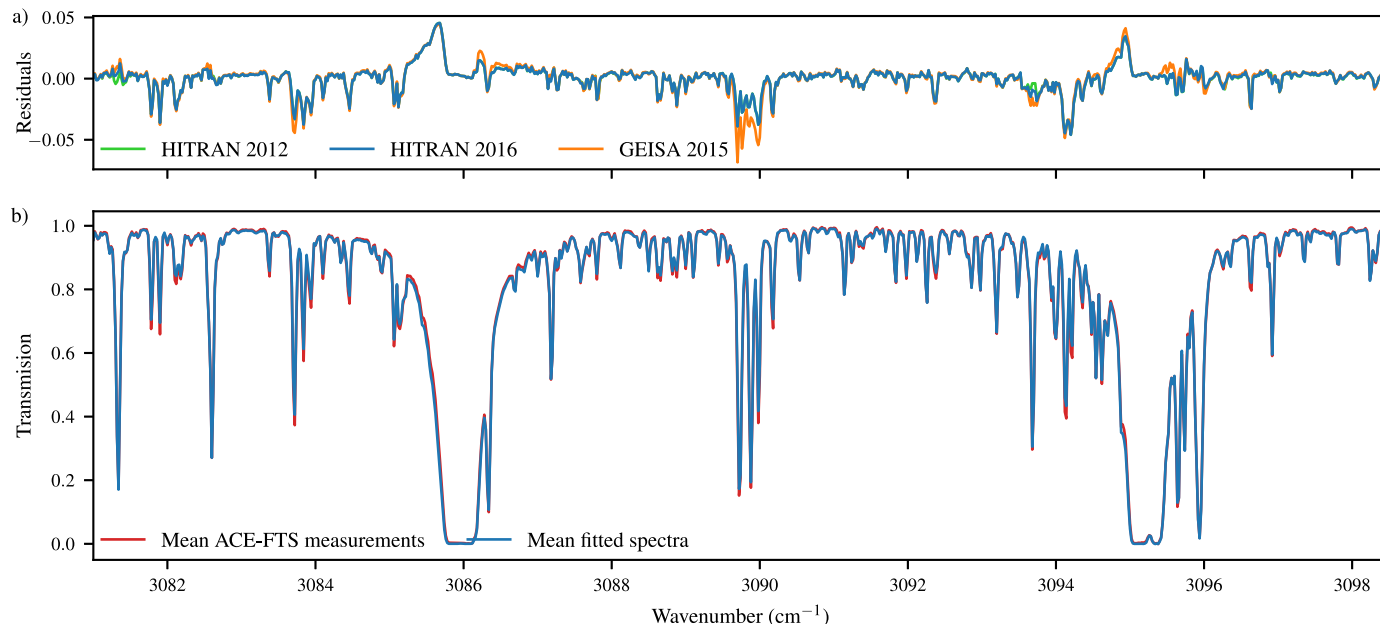


**Fig. 8.** a) Mean residuals for the 3089.75 cm<sup>-1</sup> window at 0.052 atm (~20 km) with HITRAN 2012, HITRAN 2016, and GEISA 2015. b) Mean measured ACE-FTS spectrum and mean computed spectrum (for HITRAN 2016). Absorption are due to, in order of prominence, CH<sub>4</sub>, H<sub>2</sub>O, and O<sub>3</sub>. Large residuals near 3090 cm<sup>-1</sup> are from CH<sub>4</sub> lines.

line lists are significant ( $\sim 0.002$ ) even at the highest pressure level (near 60 km), where line depths are much weaker and only extend to 0.9. Of particular interest to ExoMars is the recently observed, weak CO<sub>2</sub> band centred near 3000 cm<sup>-1</sup> that overlaps with these strong CH<sub>4</sub> features [9,67]. This band is not visible in terrestrial solar occultation observations, its lines are too weak relative to the abundant absorption features of CH<sub>4</sub> and O<sub>3</sub>.

Fig. 8 shows the mean spectra and mean residuals for fitting window 3089.75 cm<sup>-1</sup>. This region contains a set of three CH<sub>4</sub> lines near 3090 cm<sup>-1</sup> that are poorly fit with either line list. When using HITRAN 2012 and HITRAN 2016, the magnitude of the mean residuals is 0.04, which is on the order of the line mixing errors seen when fitting stronger lines. When using GEISA 2015, the mean residuals are 50% larger. Fig. 8 also shows a pair of saturated CH<sub>4</sub> lines, and fitting errors characteristic of such lines.

The window centred at 3126.65 cm<sup>-1</sup> has some of the strongest CH<sub>4</sub> lines, and, therefore, the largest residuals. GEISA 2015 and HITRAN 2016 perform similarly here. The window centred at 3202.0 cm<sup>-1</sup> contains the right edge of CH<sub>4</sub>  $\nu_2$  band. At higher wavenumbers, H<sub>2</sub>O absorption becomes dominant. This window also features overlapping CO<sub>2</sub> and O<sub>3</sub> bands, the edge of the strong CH<sub>4</sub> band, and several water vapour lines. The 3292.0 cm<sup>-1</sup> window contains H<sub>2</sub>O and CO<sub>2</sub> lines, with an H<sub>2</sub>O line strength error at 3254.15 cm<sup>-1</sup> that has been reduced between HITRAN 2012 and HITRAN 2016, but is still significant in both HITRAN 2016 and GEISA 2015. This window contains several other H<sub>2</sub>O lines where significant improvements were made to both line lists since HITRAN 2012 (e.g., at 3273.4 and 3276.5 cm<sup>-1</sup>). The 3391.15 cm<sup>-1</sup> window is similar, but hosts another set of HNO<sub>3</sub> lines missing from both line lists. There is also an H<sub>2</sub>O line strength error at 3367.65 cm<sup>-1</sup> in both GEISA 2015 and HITRAN 2016 that was not significant in HITRAN 2012.

### 6.3. 3440 – 3770 cm<sup>-1</sup>: CO<sub>2</sub>

This region was covered by five wide windows centred at 3391.15, 3489.0, 3577.0, 3665.0, and 3753.0 cm<sup>-1</sup>. These windows cover the strongest CO<sub>2</sub> vibration-rotation bands observed by the ExoMars instruments. Throughout this region, there are only small

differences between fits using GEISA 2015 and HITRAN 2016. However, there are significant improvements to several lines throughout since HITRAN 2012. Fig. 9 shows the mean spectra and residuals for the window centred at 3489.0 cm<sup>-1</sup>, where the most dramatic improvement is seen. The spectroscopic parameters for an entire band have been updated, resulting in significant improvements to fitting.

### 6.4. 3770 – 4080 cm<sup>-1</sup>: H<sub>2</sub>O

This spectral region, covered by four broad fitting windows centred at 3822.5, 3869.14, 3936.15, and 4026.0 cm<sup>-1</sup>, features the strongest set of water vapour lines in the ExoMars region of interest. It is in this region where we again find that spectral fitting with the HITRAN 2016 results in smaller residuals than when using GEISA 2015, as seen in Fig. 3. Fig. 10 shows the window centred at 3869.14 cm<sup>-1</sup>. The primary features are broad, saturated H<sub>2</sub>O lines, but there are also many smaller CH<sub>4</sub> and N<sub>2</sub>O lines, and many very weak lines from CO<sub>2</sub> and O<sub>3</sub>. The lines where fitting with GEISA 2015 resulted in systematic residual errors are largely attributable to weaker O<sub>3</sub> lines. Similar behaviour is seen in the window centred at 3822.5 cm<sup>-1</sup>, where several O<sub>3</sub> lines are not contained in GEISA 2015. Note the marked improvement in the strong H<sub>2</sub>O line between HITRAN 2012 and the newer line lists near 3886 cm<sup>-1</sup>, as shown in Fig. 6c, but clearly visible in Fig. 10.

The two windows at 3936.15 and 4026.0 cm<sup>-1</sup> show improvements over the previous two windows when comparing GEISA 2015 and HITRAN 2016. The 3936.15 cm<sup>-1</sup> window contains a portion of an O<sub>3</sub> P-branch. Significant residuals when using GEISA 2015 are from widely spaced CH<sub>4</sub> lines (e.g., at 3912.15, 3914.6, and 3914.9 cm<sup>-1</sup>), rather than O<sub>3</sub>. Two of these features near 3914.6 cm<sup>-1</sup> are shown in Fig. 6d. There is an H<sub>2</sub>O line strength error in the HITRAN 2016 line list at 3925.15 cm<sup>-1</sup> that was not present in HITRAN 2012, nor GEISA 2015. The 4026.0 cm<sup>-1</sup> window hosts an O<sub>3</sub> band, for which all line lists have difficulty accurately fitting over the region of the Q-branch. The O<sub>3</sub> band in this region is much better characterized by GEISA 2015 than that covered by the 3822.5 and 3869.14 cm<sup>-1</sup> windows, but there remain

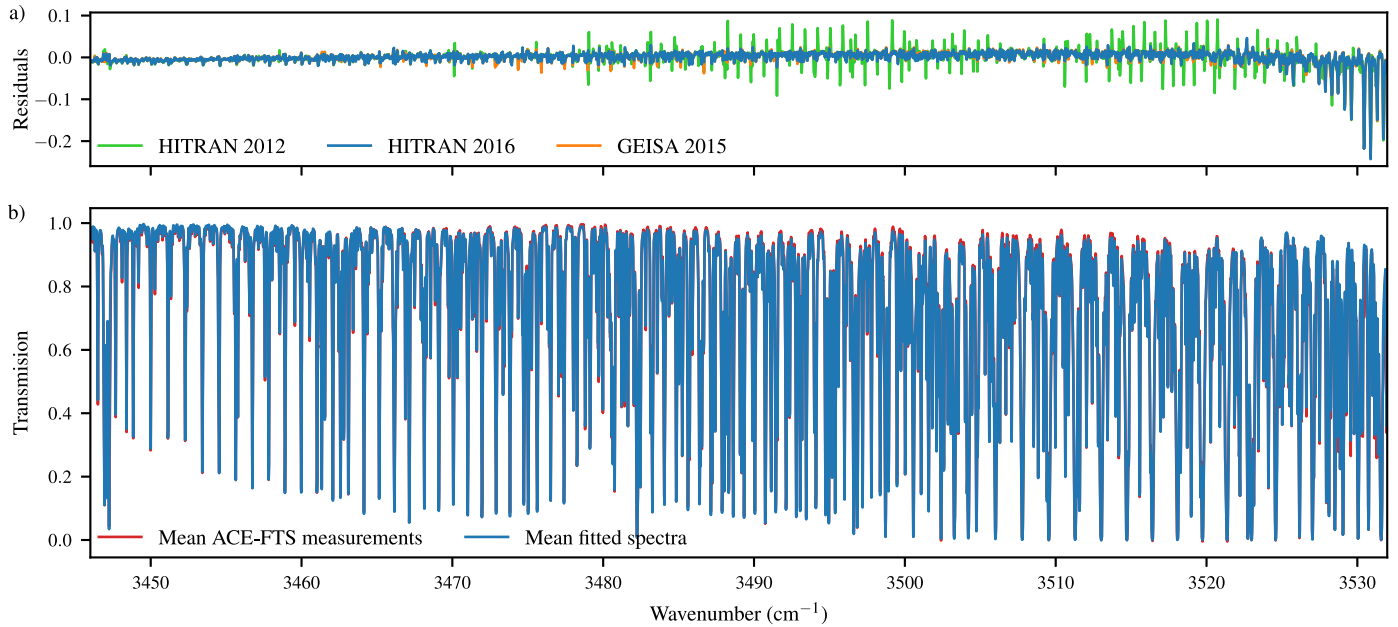


**Fig. 9.** (a) Mean residuals for the 3489.0  $\text{cm}^{-1}$  window at 0.052 atm ( $\sim 20$  km) with HITRAN 2012, HITRAN 2016, and GEISA 2015. (b) Mean measured ACE-FTS spectrum and mean computed spectrum (for HITRAN 2016). The primary features are an  $\text{N}_2\text{O}$  band on the left side,  $\text{CO}_2$  bands on the right, and several  $\text{H}_2\text{O}$  lines. The strong residuals are due to  $\text{CO}_2$  when using the HITRAN 2012 line list.

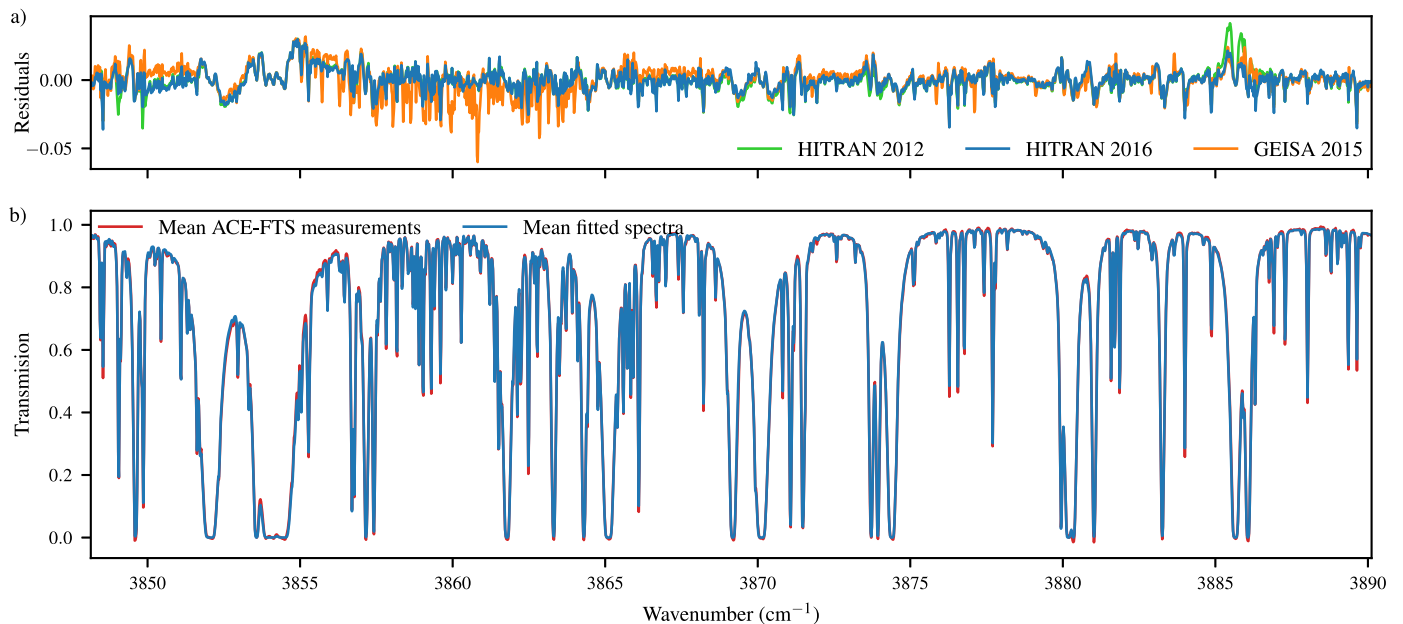


**Fig. 10.** (a) Mean residuals for the 3869.14  $\text{cm}^{-1}$  window at 0.052 atm ( $\sim 20$  km) with HITRAN 2012, HITRAN 2016, and GEISA 2015. (b) Mean measured ACE-FTS spectrum and mean computed spectrum (for HITRAN 2016). The primary features are  $\text{H}_2\text{O}$  lines. The strong residuals near 3860  $\text{cm}^{-1}$  are due to  $\text{O}_3$  when using GEISA 2015. Those near 3886  $\text{cm}^{-1}$  are due to  $\text{H}_2\text{O}$  and are shown in Fig. 6c.

small discrepancies in some minor  $\text{CH}_4$  lines, especially towards the right edge of the window at 4080.65 and 4082.8  $\text{cm}^{-1}$ .

#### 6.5. 4080 – 4420 $\text{cm}^{-1}$ : $\text{CH}_4$

Above 4100  $\text{cm}^{-1}$ , the ACE-FTS noise increases, as can be seen in Fig. 2, and it becomes difficult to evaluate the line lists further. This region is characterized by a decreasing density of  $\text{H}_2\text{O}$  lines, increasingly stronger, and more dense  $\text{CH}_4$  absorption features, and a band of broadly spaced CO lines. We evaluated five wide fitting windows in this region centred at 4132.1, 4214.2, 4300.4, 4377.0, and 4436.2  $\text{cm}^{-1}$ . At 4115.65  $\text{cm}^{-1}$ , a  $\text{CH}_4$  line missing in HITRAN

2012, as identified by Toon et al. [60], was added (also included in GEISA 2015). There are  $\text{CH}_4$  line strength errors in the GEISA 2015 line list at 4133.35  $\text{cm}^{-1}$  and 4103.2  $\text{cm}^{-1}$  that result in mean residuals on the order of 0.1 at lower pressure levels. The latter is also apparent in HITRAN 2016, despite not being present in HITRAN 2012.

As shown in Fig. 3, the mean RMS values dramatically increase in this spectral region for all evaluated line lists. At the lowest pressure level, fitting with HITRAN 2016 results in the smallest residuals and the lowest mean RMS values. It must be noted that the magnitude of the difference between results using HITRAN 2016 and GEISA 2015 is on the order of the difference between

changing pressure levels, and that is only  $\sim 1/5$  of the magnitude of the mean RMS. Therefore, errors due to differences in the spectroscopic parameters are much, much smaller than the noise level of the instrument in this region.

The window centred at  $4214.2\text{ cm}^{-1}$  features the most dramatic difference between fitting using GEISA 2015 and fitting using HITRAN 2016. Mean residuals with magnitudes greater than 0.1 come from several  $\text{CH}_4$  lines near  $4208$ ,  $4229$ , and  $4255\text{ cm}^{-1}$ .

## 7. Conclusions

This study was motivated by the release of two new editions of spectroscopic line lists, the 2015 version of GEISA and the 2016 version of HITRAN, and the launch and arrival of the ExoMars Trace Gas Orbiter as Mars, equipped with two suits of spectroscopic instruments dedicated to characterizing the Martian atmosphere. The largest efforts made recently towards updating infrared spectroscopic databases has been in support of terrestrial greenhouse gas observatories such as OCO-2, GOSAT, and TCCON. Since the Martian atmosphere is composed of 96.5%  $\text{CO}_2$ , these updates are very significant for the ExoMars mission. Our objective was to validate the two line lists in the range of  $2325\text{--}4350\text{ cm}^{-1}$  by examining spectral fitting results for terrestrial solar occultation observations made by ACE-FTS.

This work follows that of [60] who compared different versions of HITRAN, up to the 2012 release, in the spectral range of  $670\text{--}5620\text{ cm}^{-1}$  using the solar occultation measurements made by the MkIV FTS. They identified several errors in HITRAN 2012, some persisting from previous releases, and others newly introduced. The analysis in [60] is expanded in [58], which includes a detailed analysis of HITRAN 2016 using laboratory and solar occultation spectra. Because spectroscopic parameters taken from previous HITRAN versions for some gases in some spectral regions perform better, and because HITRAN may be incomplete in some spectral regions (e.g.,  $\text{HNO}_3$ ), the TCCON and GGG development teams maintain a custom line list, as do other spectroscopic analysis teams, such as ACE-FTS.

The 2016 edition of the HITRAN line list addressed several errors identified in the 2012 edition by Toon et al. [60], such as the positional error in an  $\text{O}_3$  resonance transition at  $2761.42\text{ cm}^{-1}$  (still persists in GEISA 2015). We have observed, however, a few minor errors introduced into HITRAN 2016 since the 2012 edition, such as the  $\text{H}_2\text{O}$  line strength errors at  $3367.65\text{ cm}^{-1}$  (also in GEISA 2015) and  $3925.15\text{ cm}^{-1}$ .

For ExoMars, the gases of primary interest are  $\text{CO}_2$ ,  $\text{H}_2\text{O}$ ,  $\text{CO}$ , and  $\text{CH}_4$ . Changes to line position and strength have been made to  $\text{CO}_2$  lines across our spectral region. For terrestrial spectra, the strongest improvements seen in fitting coincide with the strongest absorption features, and the greatest improvement is seen between  $3470\text{--}3530\text{ cm}^{-1}$  for both GEISA 2015 and HITRAN 2016. In no region were increased residuals seen for  $\text{CO}_2$  lines when using the updated line list editions when compared to HITRAN 2012. In the terrestrial observations, we also observe significant improvements to a subset of  $\text{H}_2\text{O}$  lines, especially at higher wavenumbers, such as near  $3093.7$  or  $3885.5\text{ cm}^{-1}$ . With the exception of individual  $\text{CH}_4$  line errors, little difference is observed in the  $\text{CH}_4$  or  $\text{CO}$  transitions in this spectral region between HITRAN 2012 and 2016.

Of key interest to us was the  $\text{CO}_2$  vibration-rotation band centred at  $2982\text{ cm}^{-1}$  and partially overlapping the critically important  $\text{CH}_4\text{ } \nu_2$  band. When comparing synthetic spectra generated with HITRAN 2016 or GEISA 2015, significant differences in these lines are seen. This band is absent from GEISA 2015, but present in HITRAN 2012 and 2016. The lines included in HITRAN 2016 have significantly increased line strengths relative to HITRAN 2012. Unfortunately, in terrestrial observations, these lines are too weak relative to interfering species, especially  $\text{CH}_4$ , and noise. It is not ob-

served in the ACE-FTS spectra examined here above background noise levels, so residuals between spectral fits using HITRAN 2012 and 2016 have not been compared.

A critical difference between the application of spectroscopic calculations for Earth and Mars is that because the Martian atmosphere is predominantly  $\text{CO}_2$  rather than  $\text{N}_2$ , the collision-induced broadening parameters computed for HITRAN and GEISA will not be applicable to the Martian atmosphere. There is ongoing work to determine spectroscopic parameters for a  $\text{CO}_2$ -rich atmosphere: e.g., [20,24] for water vapour; and [38] for  $\text{CO}$ . However, this study does not attempt to validate these parameters, nor does it evaluate the  $\text{CO}_2$  self-broadening parameters.

When comparing the 2015 version of the GEISA line list to the latest, 2016, release of HITRAN, we observe that lower RMS values are found for residuals from the majority of the spectral windows between  $2325\text{--}4350\text{ cm}^{-1}$  used here. We find that these are primarily due to differences in line strength or position for strong  $\text{O}_3$  and  $\text{CH}_4$  lines. There are some minor errors in specific lines noted as well.

We were surprised to find a large number of  $\text{O}_3$  lines missing from GEISA 2015 in the  $3830\text{--}3870\text{ cm}^{-1}$  region that were present in HITRAN 2012. The primary source of  $\text{O}_3$  lines both HITRAN 2016 and GEISA 2015 is the Spectroscopy and Molecular Properties of Ozone (S&MPO) information system [2] maintained by Reims University and the Institute of Atmospheric Optics (Toms). For GEISA 2015, new measurements of lines around this region were made at Reims University by Barbe et al. [4,6], but those lines precisely between  $3830\text{--}3870\text{ cm}^{-1}$  are attributed to a private communication from Barbe (2011).  $\text{O}_3$  line parameters in HITRAN 2016 are also included in the S&MPO database. In the region  $3623\text{--}4229\text{ cm}^{-1}$ , HITRAN also includes an updated hot band from Barbe et al. [5].

Our analysis fit the hydrogen halides  $\text{HCl}$  (between  $2600\text{--}3050\text{ cm}^{-1}$ ) and  $\text{HF}$  (between  $3700\text{--}4100\text{ cm}^{-1}$ ). Parameters for these gases were not updated in the 2011 or 2015 editions of GEISA, but new calculations were implemented in the 2012 edition of HITRAN [37]. The result is differences in line position when performing spectral fitting with HITRAN 2016 or GEISA 2015. Mean differences are very small relative to the noise of the ACE-FTS observations, less than 1%, with HITRAN 2016 performing slightly better at these line locations (e.g.,  $2925.9\text{ cm}^{-1}$  or  $2944.93\text{ cm}^{-1}$  for  $\text{HCl}$ , and  $3877.7\text{ cm}^{-1}$  or  $3920.3\text{ cm}^{-1}$  for  $\text{HF}$ ).

In conclusion, we have noted consistent improvement in both line lists since HITRAN 2012, have noted errors and deficiencies in both line lists where found, and we hope that the collaborations in charge of both line lists will find this analysis useful when compiling the next release. However, for the purposes of the ExoMars TGO ACS and NOMAD instruments, we recommend HITRAN 2016 for use. HITRAN 2016 shows marked improvement over HITRAN 2012 in  $\text{CO}_2$  and  $\text{H}_2\text{O}$  transitions (as does GEISA 2015). GEISA 2015 currently produces larger residuals for strong  $\text{CH}_4$  lines that are critical for ExoMars, while an important  $\text{CO}_2$  band centred at  $2982\text{ cm}^{-1}$  has not yet been introduced.

## Acknowledgments

All spectral fitting was performed by KSO using the GGG software suite. The ACE-FTS spectra were provided by CDB, who also provided valuable input towards their use and fitting. The GGG software suite is maintained by GCT at JPL (tcon-wiki.caltech.edu). Input on interpreting the results and the spectroscopy in the target region was provided by CDB and GCT. The HITRAN line list is hosted by the Harvard-Smithsonian Center for Astrophysics under the continued direction of Dr Laurence S. Rothman (hitran.org). The GEISA line list is compiled by the Atmospheric Radiation Analysis group at LMD and hosted by the Institut Pierre Simon Laplace (cds-espri.ipsl.upmc.fr/GEISA/geisa\_raie\_2015.php). Tools hosted by

the Earth Observation Data Group were used to reformat the GEISA 2015 line list into the format of the HITRAN line list (eodg.atm.ox.ac.uk/RFM/geihit.html). This work was performed in support of the ExoMars TGO ACS instrument and funded by the National Centre for Space Studies of France (CNES) and the Natural Sciences and Engineering Research Council of Canada (NSERC) (PDF - 516895 - 2018).

## Supplementary material

Supplementary material associated with this article can be found, in the online version, at <https://doi.org/10.1016/j.jqsrt.2019.106590>.

## References

- Armante R, Scott N, Crevoisier C, Capelle V, Crepeau L, Jacquinet N, et al. Evaluation of spectroscopic databases through radiative transfer simulations compared to observations. application to the validation of GEISA 2015 with IASI and TCCON. *J Mol Spectrosc* 2016;327:180–92. doi:10.1016/j.jms.2016.04.004.
- Babikov YL, Mikhailenko SN, Barbe A, Tyuterev VG. S&MPO - An information system for ozone spectroscopy on the web. *J Quant Spectrosc Radiat Trans* 2014;145:169–96. doi:10.1016/j.jqsrt.2014.04.024.
- Bailey J. A comparison of water vapor line parameters for modeling the venus deep atmosphere. *Icarus* 2009;201:444–53. doi:10.1016/j.icarus.2009.01.013.
- Barbe A, De Backer M-R, Starikova E, Tashkun SA, Thomas X, Tyuterev VG. FTS High resolution spectra of  $^{16}\text{O}_3$  in 3500 and 5500  $\text{cm}^{-1}$  regions. first example of new theoretical modelling for a polyad of strongly coupled states. *J Quant Spectrosc Radiat Trans* 2012;113:829–39. doi:10.1016/j.jqsrt.2012.02.034.
- Barbe A, Mikhailenko S, Starikova E, De Backer M-R, Tyuterev VG, Mondelain D, et al. Ozone spectroscopy in the electronic ground state: high-resolution spectra analyses and update of line parameters since 2003. *J Quant Spectrosc Radiat Trans* 2013;130:172–90. doi:10.1016/j.jqsrt.2013.06.007.
- Barbe A, Plateaux JJ, Mikhailenko S, Tyuterev VG. Infrared spectrum of ozone in the 4600 and 5300  $\text{cm}^{-1}$  regions: high order accidental resonances through the analysis of  $\nu_1 + 2\nu_2 + 3\nu_3 - \nu_2$ ,  $\nu_1 + 2\nu_2 + 3\nu_3$ , and  $4\nu_1 + \nu_3$  bands. *J Mol Spectrosc* 1997;185:408–16. doi:10.1006/jmsp.1997.7374.
- Barber RJ, Tennyson J, Harris GJ, Tolchenov RN. A high-accuracy computed water line list. *Mon Not R Astron Soc* 2006;368:1087–94. doi:10.1111/j.1365-2966.2006.10184.x.
- Bernath PF, McElroy CT, Abrams MC, Boone CD, Butler M, Camy-Peyret C, et al. Atmospheric chemistry experiment (ACE): mission overview. *Geophys Res Lett* 2005;32:L15S01. doi:10.1029/2005GL022386.
- Bertaux J-L, Vandaele AC, Wilquet V, Montmessin F, Dahoo R, Villard E, et al. First observation of 628  $\text{CO}_2$  isotopologue band at 3.3  $\mu\text{m}$  in the atmosphere of venus by solar occultation from venus express. *Icarus* 2008;195:28–33. doi:10.1016/j.icarus.2008.01.001.
- Birk M, Wagner G, Loos J, Lodi L, Polyansky OL, Kyuberis AA, et al. Accurate line intensities for water transitions in the infrared: comparison of theory and experiment. *J Quant Spectrosc Radiat Trans* 2017;203:88–102. doi:10.1016/j.jqsrt.2017.03.040.
- Boone CD, Nassar R, Walker KA, Rochon Y, McLeod SD, Rinsland CP, et al. Retrievals for the atmospheric chemistry experiment fourier-transform spectrometer. *Appl Opt* 2005;44:7218–31. doi:10.1364/AO.44.007218.
- Brown LR, Sung K, Benner DC, Devi VM, Boudon V, Gabard T, et al. Methane line parameters in the HITRAN2012 database. *J Quant Spectrosc Radiat Trans* 2013;130:201–19. doi:10.1016/j.jqsrt.2013.06.020.
- Chédin A, Husson N, Scott NA. GEISA - A data base for the study of phenomena of radiative transfer in planetary atmospheres. *Bulletin d'Information du Centre de Données Stellaires* 1982;22:121.
- Clarke JT, Mayyasi M, Bhattacharyya D, Schneider NM, McClintock WE, Deighan JL, et al. Variability of D and H in the martian upper atmosphere observed with the MAVEN IUVS echelle channel. *J Geophys Res* 2017;122:2336–44. doi:10.1002/2016JA023479.
- Clerbaux C, Boynard A, Clarisse L, George M, Hadji-Lazaro J, Herbin H, et al. Monitoring of atmospheric composition using the thermal infrared IASI/metop sounder. *Atmos Chem Phys* 2009;9:6041–54.
- Coudert LH, Chelin P. Line position and line intensity analyses of the high-resolution spectrum of  $\text{H}_2^{18}\text{O}$  up to the first triad and  $J = 17$ . *J Mol Spectrosc* 2016;326:130–5. doi:10.1016/j.jms.2016.01.012.
- Coudert LH, Martin-Drumel M-A, Pirali O. Analysis of the high-resolution water spectrum up to the second triad and to  $J = 30$ . *J Mol Spectrosc* 2014;303:36–41. doi:10.1016/j.jms.2014.07.003.
- Crisp D, Atlas RM, Breon F-M, Brown LR, Burrows JP, Ciaia P, et al. The orbiting carbon observatory (OCO) mission. *Adv Space Res* 2004;34:700–9. doi:10.1016/j.asr.2003.08.062.
- Crisp D, Pollock HR, Rosenberg R, Chapsky L, Lee RAM, Oyafuso FA, et al. The on-orbit performance of the orbiting carbon observatory-2 (OCO-2) instrument and its radiometrically calibrated products. *Atmos Meas Tech* 2017;10:59–81. doi:10.5194/amt-10-59-2017.
- Devi VM, Benner DC, Sung K, Crawford TJ, Gamache RR, Renaud CL, et al. Line parameters for  $\text{CO}_2$ - and self-broadening in the  $\nu_3$  band of  $\text{HD}^{16}\text{O}$ . *J Quant Spectrosc Radiat Trans* 2017;203:158–74. doi:10.1016/j.jqsrt.2017.02.020.
- Durry G, Li JS, Vinogradov I, Titov A, Joly L, Cousin J, et al. Near infrared diode laser spectroscopy of  $\text{C}_2\text{H}_2$ ,  $\text{H}_2\text{O}$ ,  $\text{CO}_2$  and their isotopologues and the application to TDLAS, a tunable diode laser spectrometer for the martian PHOBOS-GRUNT space mission. *Appl Phys B* 2010;99:339–51. doi:10.1007/s00340-010-3924-y.
- Encrenaz T, DeWitt C, Richter MJ, Greathouse TK, Fouchet T, Montmessin F, et al. New measurements of D/H on mars using EXES aboard SOFIA. *Astron Astrophys* 2018;612. doi:10.1051/0004-6361/201732367.
- Formisano V, Atreya S, Encrenaz T, Ignatiev N, Giuranna M. Detection of methane in the atmosphere of mars. *Science* 2004;306:1758–61. doi:10.1126/science.1101732.
- Gamache RR, Faresse M, Renaud CL. A spectral line list for water isotopologues in the 1100–4100  $\text{cm}^{-1}$  region for application to  $\text{CO}_2$ -rich planetary atmospheres. *J Mol Spectrosc* 2016;326:144–50. doi:10.1016/j.jms.2015.09.001.
- Giuranna M, Viscardi S, Daerden F, Neary L, Etiopie G, Oehler D, et al. Independent confirmation of a methane spike on mars and a source region east of gale crater. *Nat Geosci* 2019;17:52–10908. doi:10.1038/s41561-019-0331-9.
- Gordon IE, Rothman LS, Hill C, Kochanov RV, Tan Y, Bernath PF, et al. The HITRAN2016 molecular spectroscopic database. *J Quant Spectrosc Radiat Trans* 2017;203:3–69. doi:10.1016/j.jqsrt.2017.06.038.
- Huang X, Gamache RR, Freedman RS, Schwenke DW, Lee TJ. Reliable infrared line lists for 13  $\text{CO}_2$  isotopologues up to  $E' = 18,000 \text{ cm}^{-1}$  and 1500 K, with line shape parameters. *J Quant Spectrosc Radiat Trans* 2014;147:134–44. doi:10.1016/j.jqsrt.2014.05.015.
- Irion FW, Gunson MR, Toon GC, Chang AY, Eldering A, Mahieu E, et al. Atmospheric trace molecule spectroscopy (ATMOS) experiment version 3 data retrievals. *Appl Opt* 2002;41:6968–79. doi:10.1364/AO.41.006968.
- Jacquemart D, Gueye F, Lyulin OM, Karlovets EV, Baron D, Perevalov VI. Infrared spectroscopy of  $\text{CO}_2$  isotopologues from 2200–7000  $\text{cm}^{-1}$ : I-Characterizing experimental uncertainties of positions and intensities. *J Quant Spectrosc Radiat Trans* 2012;113:961–75. doi:10.1016/j.jqsrt.2012.02.020.
- Jacquinet-Husson N, Armante R, Scott NA, Chédin A, Crépeau L, Boutammine C, et al. The 2015 edition of the GEISA spectroscopic database. *J Mol Spectrosc* 2016;327:31–72. doi:10.1016/j.jms.2016.06.007.
- Johnson TJ, Profeta LTM, Sams RL, Griffith DWT, Yokelson RL. An infrared spectral database for detection of gases emitted by biomass burning. *Vib Spectrosc* 2010;53:97–102. doi:10.1016/j.vibspec.2010.02.010.
- Kalnay E, Kanamitsu M, Kistler R, Collins W, Deaven D, Gandin L, et al. The NCEP/NCAR 40-Year reanalysis project. *Bull Am Astron Soc* 1996;77:437–72. doi:10.1175/1520-0477(1996)077<0437:TNYRP>2.0.CO;2.
- Korablev O, Montmessin F, Trokhimovskiy A, Fedorova AA, Shakun AV, Grigoriev AV, et al. The atmospheric chemistry suite (ACS) of three spectrometers for the exomars 2016 trace gas orbiter. *Space Sci Rev* 2018;214. doi:10.1007/s11214-017-0437-6.
- Korablev O, Vandaele AC, Montmessin F, Fedorova AA, Trokhimovskiy A, Forget F, et al. No detection of methane on mars from early exomars trace gas orbiter observations. *Nature* 2019. doi:10.1038/s41586-019-1096-4.
- Krasnopolsky VA. Variations of the  $\text{HDO}/\text{H}_2\text{O}$  ratio in the martian atmosphere and loss of water from mars. *Icarus* 2015;257:377–86. doi:10.1016/j.icarus.2015.05.021.
- Krasnopolsky VA, Maillard JP, Owen TC. Detection of methane in the martian atmosphere: evidence for life? *Icarus* 2004;172:537–47. doi:10.1016/j.icarus.2004.07.004.
- Li G, Gordon IE, Hajigeorgiou PG, Coxon JA, Rothman LS. Reference spectroscopic data for hydrogen halides, part II: the line lists. *J Quant Spectrosc Radiat Trans* 2013;130:284–95. doi:10.1016/j.jqsrt.2013.07.019.
- Li G, Gordon IE, Rothman LS, Tan Y, Hu S-M, Kassi S, et al. Rovibrational line lists for nine isotopologues of the CO molecule in the  $X^1\Sigma^+$  ground electronic state. *Astrophys J Suppl Ser* 2015;216. doi:10.1088/0067-0049/216/1/15.
- Lodi L, Tennyson J. Line lists for  $\text{H}_2^{18}\text{O}$  and  $\text{H}_2^{17}\text{O}$  based on empirical line positions and ab initio intensities. *J Quant Spectrosc Radiat Trans* 2012;113:850–8. doi:10.1016/j.jqsrt.2012.02.023.
- Lodi L, Tennyson J, Polyansky OL. A global, high accuracy ab initio dipole moment surface for the electronic ground state of the water molecule. *J Chem Phys* 2011;135(3):034113. doi:10.1063/1.3604934.
- Loos J, Birk M, Wagner G. Measurement of air-broadening line shape parameters and temperature dependence parameters of  $\text{H}_2\text{O}$  lines in the spectral ranges 1850–2280  $\text{cm}^{-1}$  and 2390–4000  $\text{cm}^{-1}$ . *J Quant Spectrosc Radiat Trans* 2017a;203:103–18. doi:10.1016/j.jqsrt.2017.03.033.
- Loos J, Birk M, Wagner G. Measurement of positions, intensities and self-broadening line shape parameters of  $\text{H}_2\text{O}$  lines in the spectral ranges 1850–2280  $\text{cm}^{-1}$  and 2390–4000  $\text{cm}^{-1}$ . *J Quant Spectrosc Radiat Trans* 2017b;203:119–32. doi:10.1016/j.jqsrt.2017.02.013.
- Lyulin OM, Karlovets EV, Jacquemart D, Lu Y, Liu AW, Perevalov VI. Infrared spectroscopy of  $^{17}\text{O}$ - and  $^{18}\text{O}$ -enriched carbon dioxide in the 1700–8300  $\text{cm}^{-1}$  wavenumber region. *J Quant Spectrosc Radiat Trans*. 2012;113:2167–81. doi:10.1016/j.jqsrt.2012.06.028.
- McClatchey RA, Benedict WS, Clough SA, Burch DE, Calfee RF, Fox K, et al. AFCRL atmospheric absorption line parameters compilation. Bedford, Ma: Air Force Cambridge Research Laboratories; 1973.
- Mendonça J, Strong K, Toon GC, Wunch D, Sung K, Deutscher NM, et al. Improving atmospheric  $\text{CO}_2$  retrievals using line mixing and speed-dependence

- when fitting high-resolution ground-based solar spectra. *J Mol Spectrosc* 2016;323:15–27. doi:10.1016/j.jms.2016.01.007.
- [46] Mumma MJ, Villanueva GL, Novak RE, Hewagama T, Bonev BP, DiSanti MA, et al. Strong release of methane on mars in northern summer. *Science* 2009;323:1041–5. doi:10.1126/science.1165243.
- [47] Niederer H-M, Wang X-G, Carrington T, Albert S, Bauerecker S, Boudon V, et al. Analysis of the rovibrational spectrum of  $^{13}\text{CH}_4$  in the octad range. *J Mol Spectrosc* 2013;291:33–47. doi:10.1016/j.jms.2013.06.003.
- [48] Nikitin AV, Boudon V, Wenger C, Albert S, Brown LR, Bauerecker S, et al. High resolution spectroscopy and the first global analysis of the tetradecad region of methane  $^{12}\text{CH}_4$ . *Phys Chem Chem Phys* 2013;15:10071. doi:10.1039/C3CP50799H.
- [49] Norton RH, Rinsland CP. ATMOS Data processing and science analysis methods. *Appl Opt* 1991;30:389–400. doi:10.1364/AO.30.000389.
- [50] Olsen KS, Toon GC, Boone CD, Strong K. New temperature and pressure retrieval algorithm for high-resolution infrared solar occultation spectrometry: analysis and validation against ACE-FTS and COSMIC. *Atmos Meas Tech Disc* 2015;8:10823–73. doi:10.5194/amt-d-8-10823-2015.
- [51] Rothman LS, Gamache RR, Tipping RH, Rinsland CP, Smith MAH, Benner DC, et al. The HITRAN molecular data base - Editions of 1991 and 1992. *J Quant Spectrosc Radiat Trans* 1992;48:469–507. doi:10.1016/0022-4073(92)90115-K.
- [52] Rothman LS, Gordon IE, Babikov Y, Barbe A, Chris Benner D, Bernath PF, et al. The HITRAN2012 molecular spectroscopic database. *J Quant Spectrosc Radiat Trans* 2013;130:4–50. doi:10.1016/j.jqsrt.2013.07.002.
- [53] Rothman LS, Gordon IE, Barbe A, Benner DC, Bernath PF, Birk M, et al. The HITRAN 2008 molecular spectroscopic database. *J Quant Spectrosc Radiat Trans* 2009;110:533–72. doi:10.1016/j.jqsrt.2009.02.013.
- [54] Sen B, Toon GC, Blavier J-F, Fleming EL, Jackman CH. Balloon-borne observations of midlatitude fluorine abundance. *J Geophys Res* 1996;101:9045–54. doi:10.1029/96JD00227.
- [55] Sharpe SW, Johnson TJ, Sams RL, Chu PM, Rhoderick GC, Johnson PA. Gas-Phase databases for quantitative infrared spectroscopy. *Appl Spectrosc* 2004;58:1452–61. doi:10.1366/0003702042641281.
- [56] Tashkun SA, Perevalov VI, Gamache RR, Lamouroux J. CDS-296, High resolution carbon dioxide spectroscopic databank: version for atmospheric applications. *J Quant Spectrosc Radiat Trans* 2015;152:45–73. doi:10.1016/j.jqsrt.2014.10.017.
- [57] Tennyson J, Bernath PF, Brown LR, Campargue A, Carleer MR, Császár AG, et al. IUPAC Critical evaluation of the rotational-vibrational spectra of water vapor. part I—Energy levels and transition wavenumbers for  $\text{H}_2^{17}\text{O}$  and  $\text{H}_2^{18}\text{O}$ . *J Quant Spectrosc Radiat Trans* 2009;110:573–96. doi:10.1016/j.jqsrt.2009.02.014.
- [58] Toon GC.  $\text{CO}_2$  Spectroscopy Evaluation: 670–7000  $\text{cm}^{-1}$ . Technical Report. Jet Propulsion Laboratory; 2019. [mark4sun.jpl.nasa.gov/toon/atm18/NDACC\\_TCCON\\_2019\\_Toon-compressed.pdf](http://mark4sun.jpl.nasa.gov/toon/atm18/NDACC_TCCON_2019_Toon-compressed.pdf).
- [59] Toon GC. The JPL mkiv interferometer. *Opt Photonics News* 1991;2:19–21. doi:10.1364/OPN.2.10.000019.
- [60] Toon GC, Blavier J-F, Sung K, Rothman LS, E Gordon I. HITRAN Spectroscopy evaluation using solar occultation FTIR spectra. *J Quant Spectrosc Radiat Trans* 2016;182:324–36. doi:10.1016/j.jqsrt.2016.05.021.
- [61] Toth RA, Brown LR, Miller CE, Malathy Devi V, Benner DC. Spectroscopic database of  $\text{CO}_2$  line parameters: 4300–7000  $\text{cm}^{-1}$ . *J Quant Spectrosc Radiat Trans* 2008a;109:906–21. doi:10.1016/j.jqsrt.2007.12.004.
- [62] Toth RA, Miller CE, Brown LR, Devi VM, Benner DC. Line positions and strengths of  $^{16}\text{O}^{12}\text{C}^{18}\text{O}$ ,  $^{18}\text{O}^{12}\text{C}^{18}\text{O}$  and  $^{17}\text{O}^{12}\text{C}^{18}\text{O}$  between 2200–7000  $\text{cm}^{-1}$ . *J Mol Spectrosc* 2007;243:43–61. doi:10.1016/j.jms.2007.03.005.
- [63] Toth RA, Miller CE, Brown LR, Devi VM, Benner DC. Line strengths of  $^{16}\text{O}^{13}\text{C}^{16}\text{O}$ ,  $^{16}\text{O}^{13}\text{C}^{18}\text{O}$ ,  $^{16}\text{O}^{13}\text{C}^{17}\text{O}$  and  $^{18}\text{O}^{13}\text{C}^{18}\text{O}$  between 2200 and 6800  $\text{cm}^{-1}$ . *J Mol Spectrosc* 2008b;251:64–89. doi:10.1016/j.jms.2008.01.009.
- [64] Tyuterev V, Tashkun S, Rey M, Kochanov R, Nikitin A, Delahaye T. Accurate spectroscopic models for methane polyads derived from a potential energy surface using high-order contact transformations. *J Phys Chem A* 2013;117:13779–805. doi:10.1021/jp408116j.
- [65] Vandaele AC, Lopez-Moreno J-J, Patel MR, Bellucci G, Daerden F, Ristic B, et al. NOMAD, An integrated suite of three spectrometers for the exomars trace gas mission: technical description, science objectives and expected performance. *Space Sci Rev* 2018;214. doi:10.1007/s11214-018-0517-2.
- [66] Vandaele AC, Neefs E, Drummond R, Thomas IR, Daerden F, Lopez-Moreno J-J, et al. Science objectives and performances of NOMAD, a spectrometer suite for the exomars TGO mission. *Planet Space Sci* 2015;119:233–49. doi:10.1016/j.pss.2015.10.003.
- [67] Villanueva GL, Mumma MJ, Novak RE, Hewagama T. Identification of a new band system of isotopic  $\text{CO}_2$  near 3.3  $\mu\text{m}$ : implications for remote sensing of biomarker gases on mars. *Icarus* 2008;195:34–44. doi:10.1016/j.icarus.2007.11.014.
- [68] Webster CR, Mahaffy PR, Atreya SK, Flesch GJ, Mischna MA, Meslin P-Y, et al. Mars methane detection and variability at gale crater. *Science* 2015;347:415–17. doi:10.1126/science.1261713.
- [69] Webster CR, Mahaffy PR, Atreya SK, Moores JE, Flesch GJ, Malespin C, et al. Background levels of methane in Mars' atmosphere show strong seasonal variations. *Science* 2018;360:1093–6. doi:10.1126/science.aag0131.
- [70] Wilzewski JS, Gordon IE, Kochanov RV, Hill C, Rothman LS.  $\text{H}_2$ , He, and  $\text{CO}_2$  line-broadening coefficients, pressure shifts and temperature-dependence exponents for the HITRAN database. part 1:  $\text{SO}_2$ ,  $\text{NH}_3$ , HF, HCl, OCS and  $\text{C}_2\text{H}_2$ . *J Quant Spectrosc Radiat Trans* 2016;168:193–206. doi:10.1016/j.jqsrt.2015.09.003.
- [71] Wunch D, Toon GC, Blavier JL, Washenfelder RA, Notholt J, Connor BJ, et al. The total carbon column observing network. *Phil Trans R Soc A* 2011;369:2087–112. doi:10.1098/rsta.2010.0240.
- [72] Yokota T, Yoshida Y, Eguchi N, Ota Y, Tanaka T, Watanabe H, et al. Global concentrations of  $\text{CO}_2$  and  $\text{CH}_4$  retrieved from gosat: first preliminary results. *Sci Online Lett Atmos* 2009;5:160–3. doi:10.2151/sola.2009-041.
- [73] Zak E, Tennyson J, Polyansky OL, Lodi L, Zobov NF, Tashkun SA, et al. A room temperature  $\text{CO}_2$  line list with ab-initio computed intensities. *J Quant Spectrosc Radiat Trans* 2016;177:31–42. doi:10.1016/j.jqsrt.2015.12.022.
- [74] Zurek RW, Chicarro A, Allen MA, Bertaux J-L, Clancy RT, Daerden F, et al. Assessment of a 2016 mission concept: the search for trace gases in the atmosphere of mars. *Planet Space Sci* 2011;59:284–91. doi:10.1016/j.pss.2010.07.007.